



Published in final edited form as:

Cell Rep. 2021 December 14; 37(11): 110106. doi:10.1016/j.celrep.2021.110106.

## Cholinergic feedback to bipolar cells contributes to motion detection in the mouse retina

Chase B. Hellmer<sup>1,3</sup>, Leo M. Hall<sup>1,4</sup>, Jeremy M. Bohl<sup>1</sup>, Zachary J. Sharpe<sup>1</sup>, Robert G. Smith<sup>2</sup>, Tomomi Ichinose<sup>1,5,\*</sup>

<sup>1</sup>Department of Ophthalmology, Visual and Anatomical Sciences, Wayne State University School of Medicine, Detroit, MI 48201, USA

<sup>2</sup>Department of Neuroscience, University of Pennsylvania, Philadelphia, PA 19104, USA

<sup>3</sup>Present address: Department of Ophthalmology and Visual Sciences, University of Louisville, Louisville, KY 40202, USA

<sup>4</sup>Present address: Department of Internal Medicine, St. Mary Mercy Livonia Hospital, Livonia, MI 48154, USA

<sup>5</sup>Lead contact

### SUMMARY

Retinal bipolar cells are second-order neurons that transmit basic features of the visual scene to postsynaptic partners. However, their contribution to motion detection has not been fully appreciated. Here, we demonstrate that cholinergic feedback from starburst amacrine cells (SACs) to certain presynaptic bipolar cells via alpha-7 nicotinic acetylcholine receptors ( $\alpha 7$ -nAChRs) promotes direction-selective signaling. Patch clamp recordings reveal that distinct bipolar cell types making synapses at proximal SAC dendrites also express  $\alpha 7$ -nAChRs, producing directionally skewed excitatory inputs. Asymmetric SAC excitation contributes to motion detection in On-Off direction-selective ganglion cells (On-Off DSGCs), predicted by computational modeling of SAC dendrites and supported by patch clamp recordings from On-Off DSGCs when bipolar cell  $\alpha 7$ -nAChRs is eliminated pharmacologically or by conditional knockout. Altogether, these results show that cholinergic feedback to bipolar cells enhances direction-selective signaling in postsynaptic SACs and DSGCs, illustrating how bipolar cells provide a scaffold for postsynaptic microcircuits to cooperatively enhance retinal motion detection.

This is an open access article under the CC BY-NC-ND license (<http://creativecommons.org/licenses/by-nc-nd/4.0/>).

\*Correspondence: [tichinos@med.wayne.edu](mailto:tichinos@med.wayne.edu).

#### AUTHOR CONTRIBUTIONS

Conceptualization, C.B.H. and T.I.; methodology, C.B.H., L.M.H., J.M.B., R.G.S., and T.I.; software, R.G.S.; formal analysis, C.B.H., J.M.B., R.G.S., and T.I.; investigation, C.B.H., L.M.H., J.M.B., Z.J.S., R.G.S., and T.I.; writing – original draft, C.B.H. and T.I.; writing – review & editing, C.B.H., L.M.H., J.M.B., R.G.S., and T.I.; supervision, T.I.

#### DECLARATION OF INTERESTS

The authors declare no competing interests.

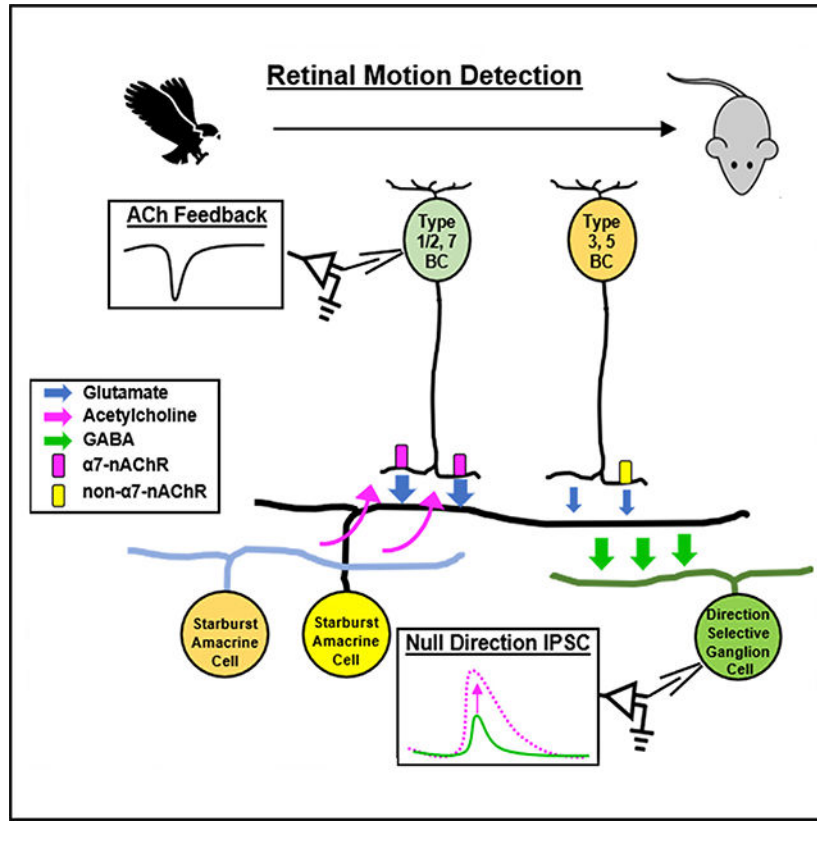
#### SUPPLEMENTAL INFORMATION

Supplemental information can be found online at <https://doi.org/10.1016/j.celrep.2021.110106>.

## In brief

Moving objects are sensed by the retina, which depends on neural circuits for visual motion detection. Hellmer et al. demonstrate that specific second-order retinal bipolar cells receive cholinergic feedback via nicotinic acetylcholine receptors, which enhances directional signaling of postsynaptic neurons in motion detection circuits.

## Graphical Abstract



## INTRODUCTION

Various features of the visual world are encoded by specific types of neurons and networks in the retina. Motion detection is an essential visual feature, which has been attributed to direction-selective ganglion cells (DSGCs) and their upstream neurons, the starburst amacrine cells (SACs). DSGCs fire action potentials for objects moving in a “preferred” direction but do not respond to objects moving in the opposite “null” direction. This direction selectivity is dependent upon SACs, critical neurons for retinal motion detection that exhibit direction-selective release of GABA and form an asymmetric inhibitory receptive field surround for DSGCs (Briggman et al., 2011; Barlow et al., 1964; Taylor and Vaney, 2002; Yoshida et al., 2001). Directional GABA release from SACs originates in their radial dendrites, in which multiple mechanisms are thought to contribute to enhanced depolarization for objects moving centrifugally, from the SAC soma toward the distal dendrites (Lee and Zhou, 2006; Vlasits et al., 2016; Kim et al., 2014; Hausselt et al., 2007;

Tukker et al., 2004; Ding et al., 2016; Euler et al., 2002). However, the contribution of upstream bipolar cells to direction selectivity remains controversial.

In this study, we focused on the contribution of bipolar cells to direction-selective signaling in the retina. Bipolar cells are second-order relay neurons that receive direct inputs from photoreceptors. Several studies concluded that bipolar cells themselves do *not* have direction selectivity and, thus, do not contribute to direction-selective signaling of postsynaptic SACs and On-Off DSGCs (Pei et al., 2015; Park et al., 2014; Yonehara et al., 2013; Chen et al., 2014). Nevertheless, recent connectomic studies showed that distinct types of bipolar cells provide excitatory synaptic inputs at different sections of the SAC dendrites. For Off-SACs, type-1 and -2 bipolar cells provide synaptic inputs at the proximal dendrites, whereas type-3 bipolar cells contact at the more-distal regions of SAC dendrites (Kim et al., 2014; Ding et al., 2016). For On-SACs, type-7 bipolar cells provide synaptic inputs at their proximal dendrites, whereas type-5 bipolar cells provide inputs at more-distal dendrites (Greene et al., 2016; Ding et al., 2016). Correspondingly, we recently found that  $\alpha 7$  nicotinic acetylcholine receptors ( $\alpha 7$ -nAChRs) are expressed in types-1, -2, and -7 bipolar cells (Hall et al., 2019), which provide glutamatergic excitatory synaptic inputs at the proximal dendrites of SACs. In addition to GABA, SACs also release acetylcholine (ACh) and are the only cholinergic neurons in the retina (Famiglietti, 1983; Yan et al., 2020; Hayden et al., 1980). Because presynaptic  $\alpha 7$ -nAChRs are known to facilitate transmitter release (McGehee et al., 1995; Alkondon et al., 1996), we examined the hypothesis that targeted cholinergic enhancement of bipolar cell inputs at the SAC proximal dendrites contributes to their direction selective signaling.

In this study, we found that bipolar cells indeed receive cholinergic feedback from SACs through either  $\alpha 7$ -nAChRs or non- $\alpha 7$ -nAChRs in a cell-type-dependent manner. When we recorded from postsynaptic On-Off DSGCs, we found that  $\alpha 7$ -nAChRs, but not non- $\alpha 7$ -nAChRs, in bipolar cells enhanced feedforward inhibition from SACs to DSGCs, therefore, having a role in their direction selectivity. Although it remains controversial whether bipolar cells themselves exhibit direction selectivity (Matsumoto et al., 2020; Pei et al., 2015; Park et al., 2014; Yonehara et al., 2013; Chen et al., 2014; Strauss et al., 2021), we propose a mechanism in which cholinergic feedback from SACs to bipolar cells and bipolar cells' type-dependent distributions to SAC dendrites enhance retinal motion detection.

## RESULTS

### Transgenic SACs express ChR2-EYFP that is activated by high-intensity, 500-nm light

We previously found that  $\alpha 7$ -nAChRs are expressed by mouse retinal bipolar cells in a type-dependent manner (Hall et al., 2019). Similarly, expression of both  $\alpha 7$ -nAChRs and non- $\alpha 7$ -nAChRs in bipolar cells has been reported (Shekhar et al., 2016; Siegert et al., 2009; Dmitrieva et al., 2007). However, it is not known whether these bipolar cells receive direct cholinergic feedback from SACs. Therefore, we used optogenetic control of SACs to examine cholinergic synaptic inputs in bipolar cells by generating mice in which SACs express Channelrhodopsin 2 (ChR2) conjugated with YFP (see Method details). We examined whether SACs in these mice correctly express ChR2 using immunohistochemistry. Both retinal wholemount and slice preparations were labeled with an

anti-choline acetyltransferase (anti-ChAT) antibody that labels On- and Off-SACs. We found that in the wholemount retina, 511/514 YFP<sup>+</sup> cells were co-labeled with anti-ChAT without ectopic expression. These included both On-SACs in the ganglion cell layer (Figure S1A) as well as Off-SACs in the inner nuclear layer (Figure S1B). In retinal slices we similarly found that 58/58 YFP cells were co-labeled with anti-ChAT (data not shown). Thus, immunolabeling confirmed that SACs exclusively and reliably express ChR2, allowing for optogenetic control of cholinergic signaling.

We also conducted whole-cell patch-clamp recordings from SACs in the wholemount retina to determine the stimulus threshold required for ChR2 activation. Photoreceptor-driven light responses in SACs were blocked by the application of AMPA/kainate glutamate receptor antagonists and an mGluR6 agonist (50  $\mu$ M GYKI53655, 1  $\mu$ M ACET, and 10  $\mu$ M L-AP4), which block the transmission from photoreceptors to Off and On bipolar cells, respectively. Subsequently, current clamp recordings were made from five On-SACs, which showed a relatively hyperpolarized resting potential in the absence of photoreceptor inputs ( $-77.3 \pm 3.4$  mV). To test ChR2-evoked SAC depolarization, we presented a 1-s step-light at increasing intensities in the high-photopic range. SACs were maximally depolarized by ChR2-activation at stimuli of  $1.56 \times 10^{10}$  photons/ $\mu$ m<sup>2</sup>/s ( $29.5 \pm 3$  mV; Figures S1C and S1D). This intensity was used for optogenetic SAC depolarization during subsequent bipolar cell recordings. Thus, we showed that in the Chat-Cre  $\times$  Ai32 retina SACs express ChR2 with high fidelity and can be isolated from photoreceptor inputs for direct optogenetic control.

Furthermore, we verified that photoreceptor inputs were absent during the higher-intensity stimulus. We recorded from bipolar cells, and a 565-nm step-light was applied at the same intensity as that used for the ChR2-stimulus, which can stimulate photoreceptors but is outside the spectral sensitivity of ChR2 (Nagel et al., 2003; Wang et al., 2011; Nikonov et al., 2006). After photoreceptor blockade, the 565-nm stimulus never evoked excitatory postsynaptic currents (EPSCs;  $n = 27$  cells, data not shown), confirming that the high-intensity, stimulus-evoked currents (Figure 1A) were attributable to ChR2.

### **ChR2-evoked EPSCs in bipolar cells were mediated by MLA or HEX-sensitive nAChRs**

Using the ChR2-SAC mouse model, we performed whole-cell patch-clamp recordings from 84 On and Off bipolar cells in the wholemount retina to examine whether bipolar cells receive cholinergic synaptic inputs from SACs. At first, a step-light stimulus at an intensity of  $1.0 \times 10^7$  photons/ $\mu$ m<sup>2</sup>/s was used to record photoreceptor-mediated EPSCs. Then, a cocktail of photoreceptor antagonists was applied in the bath. After the photoreceptor-mediated EPSCs were eliminated, ChR2-evoked EPSCs were evoked by a higher-intensity light stimulus ( $1.56 \times 10^{10}$  photons/ $\mu$ m<sup>2</sup>/s; Figure 1A, left).

We then determined whether ChR2-evoked currents were mediated by  $\alpha$ 7-nAChRs or non- $\alpha$ 7-nAChRs by application of 100  $\mu$ M methyllycaconitine (MLA) and 100  $\mu$ M hexamethonium (HEX), respectively. These blockers were applied in random order. After photoreceptor inputs were blocked, we observed that 39 of 84 bipolar cells exhibited ChR2-evoked EPSCs. All 39 EPSCs were sensitive to either MLA or HEX. In 19 of 39 bipolar cells, ChR2-evoked EPSCs were abolished by MLA but were insensitive to HEX, indicating

that they were mediated by  $\alpha 7$ -nAChRs (Figure 1). This group included both Off and On bipolar cells of multiple types (see below). MLA-sensitive EPSCs were transient relative to the 1-s optogenetic stimulus, with a half width of  $\sim 100$  ms (Table S1). In contrast, the rest of Chr2-current-evoked cells ( $n = 20$ ) were blocked by HEX perfusion but were insensitive to MLA (Figure 2). This group also included multiple types of both Off and On bipolar cells (see below). The HEX-sensitive EPSCs in these cells were mediated by non- $\alpha 7$ -nAChRs, which similarly exhibited transient signaling (Table S1). These findings demonstrate that SACs provide cholinergic feedback to individual bipolar cells, either through  $\alpha 7$ -nAChRs or non- $\alpha 7$ -nAChRs.

We analyzed whether  $\alpha 7$ -nAChRs (MLA-sensitive) and non- $\alpha 7$ -nAChRs (HEX-sensitive) were expressed by bipolar cells in a type-dependent manner. Mouse bipolar cells consist of more than 13 types, based on the axon ramification patterns in the inner plexiform layer (IPL) and molecular expressions (Figure 3A) (Wässle et al., 2009; Helmstaedter et al., 2013; Shekhar et al., 2016). To determine the types of bipolar cells in the retinal wholemount preparations, we filled bipolar cells with sulforhodamine B during recording, and the stratification depth of their axon terminals was compared with YFP-labeled ChAT bands in the IPL (Figures 3B and S2). Four different types of bipolar cells were distinguished based on their axon terminal stratification in relation to the On and Off ChAT bands (type 1/2: in focus to Off ChAT; type 3: inner to Off ChAT; type 5: in focus to On ChAT; and type 7: inner to On ChAT) (Figure S2). We found that most type 1/2 ( $n = 5/9$ ) and type 7 ( $n = 6/6$ ) bipolar cells exhibited Chr2-evoked EPSCs that were MLA sensitive (Figure 3C). The results are consistent with our previous observations that these types express  $\alpha$ -bungarotoxin-sensitive  $\alpha 7$ -nAChRs (Hall et al., 2019). In contrast, types 3 and 5 bipolar cells exhibited different features. More than half of these types did not express nAChRs. The other half of type 3 bipolar cells exhibited Chr2-evoked EPSCs that were HEX sensitive ( $n = 6/15$ ). Because type 3 cells are divided into types 3a and 3b cells (Mataruga et al., 2007; Wässle et al., 2009), our data suggest that one of the 3a or 3b cells is the HEX-sensitive type. The type-5 cells were divided into three categories: no Chr2 response (60%,  $n = 28/47$ ), HEX sensitive (25%,  $n = 12/47$ ), and MLA sensitive (15%,  $n = 7/47$ ). This diversity is likely attributable to the fact that type-5 bipolar cells consist of multiple subsets (Hellmer et al., 2016; Fyk-Kolodziej and Pourcho, 2007; Helmstaedter et al., 2013; Shekhar et al., 2016). As a whole, we found that the expression of nAChRs in type-3 and type-5 bipolar cells were similar to each other, in which subsets expressed non- $\alpha 7$ -nAChRs but most exhibited no cholinergic feedback. We also encountered individual type-1/2, type-4, and type-6 bipolar cells that exhibited Chr2-evoked EPSCs sensitive to HEX. Lastly, we did not observe Chr2-evoked EPSCs in rod bipolar cells ( $n = 4$ ), which was expected because they have not been shown to express nAChRs (Hall et al., 2019).

Subsequently, we examined the kinetics of Chr2-evoked EPSCs (Table S1). There were no significant differences in the amplitude of Chr2-evoked EPSCs from  $\alpha 7$ -nAChRs or non- $\alpha 7$ -nAChRs across all MLA- or HEX-sensitive bipolar cells ( $p = 0.38$ ; Table S1), or between bipolar cell types ( $p > 0.5$ ), indicating the conductance of nAChRs is similar in each type. We also did not detect differences in either the rise time or the half-width of MLA-sensitive EPSCs compared with HEX-sensitive EPSCs ( $p > 0.5$ ; Table S1). These results were unexpected because responses evoked by  $\alpha 7$ -nAChRs are characterized

by especially fast rise times and rapid desensitization relative to other nAChR types (Albuquerque et al., 2009). Nonetheless, the expression of either  $\alpha 7$ -nAChRs or non- $\alpha 7$ -nAChRs exclusively in different bipolar types likely still mediates differential feedback to each type (see Discussion). Altogether, we found that at least five types of bipolar cells receive direct cholinergic feedback from SACs mediated by diverse nAChR expression.

### **Cholinergic feedback to bipolar cells contributes to direction selectivity in a SAC model**

Our finding that SACs provide cholinergic feedback to multiple presynaptic bipolar cell types suggested that enhancement of glutamatergic inputs to the SAC dendrites would affect their direction selectivity. We conducted a computational simulation of SAC direction selectivity in a three-SAC model that enabled us to predict the voltage and calcium responses at any point in the SACs (Figures 4A and 4B). Biophysical models of individual SACs were based on the digitized morphology of a tracer-labeled mouse SAC, and the SAC-membrane properties were based on experimentally measured parameters from a previous study (Stincic et al., 2016). Moreover, previous reports indicate that SACs release both ACh and GABA from the distal one-third of their dendrites, which may occur from different release sites (Lee et al., 2010), and neighboring SACs also provide lateral GABAergic inhibition between antiparallel dendrites (Lee and Zhou, 2006) at postsynaptic loci proximal to the soma (Ding et al., 2016). Consequently, we arranged the spacing between neighboring SACs such that GABAergic inhibition reached the proximal dendrites of the central SAC, whereas ACh release from their distal tips reached bipolar cells on the opposite side of the central SAC soma.

Subsequently, we modeled the excitatory postsynaptic potential (EPSP) and calcium response in the right-facing dendrites of the central SAC in response to a simulated bar moving at 600  $\mu\text{m/s}$  in either direction (Figure 4B, point 1). When cholinergic feedback to bipolar cells was excluded, we observed that centrifugal motion, from left to right, evoked EPSPs and calcium responses that were greater than that of centripetal motion, from right to left. Despite exhibiting weak direction selectivity for centrifugal motion, small EPSPs in either direction were below the threshold for robust activation of voltage-gated calcium channels (Figure 4C). When excitatory cholinergic feedback to presynaptic bipolar cells was included, the moving bar stimulus evoked larger EPSPs and robust calcium channel activation for the centrifugal motion, whereas lateral GABA inhibition and dendritic electrotonic delay were sufficient to attenuate signal backpropagation from small EPSPs and less calcium channel activation for the centripetal motion (Figure 4D). Thus, computational modeling revealed that cholinergic feedback from SACs to presynaptic bipolar cells could enhance their centrifugal direction selectivity in SAC dendrites.

### **Blocking $\alpha 7$ -nAChRs reduces SAC feedforward inhibition to On-Off DSGCs**

To examine the function of cholinergic feedback to bipolar cells, we recorded light-evoked inhibitory postsynaptic currents (L-IPSCs) from On-Off DSGCs to moving bars and pharmacologically assessed the nAChR contributions. IPSCs were recorded at a membrane potential of 0 mV, in which nAChRs are rectified and nulled (Alkondon and Albuquerque, 1993; Sethuramanujam et al., 2016). Because SACs do not express nAChRs (Hall et al.,

2019), if the application of nAChR antagonists changed the L-IPSCs, the site of the antagonists' action should be presynaptic to the DSGCs, including bipolar cells.

We recorded L-IPSCs from a DSGC in response to moving light stimuli of eight directions in control solution, which showed larger IPSCs in the DSGC's null direction than its preferred direction (Figure 5A). We applied HEX in the bath solution to block non- $\alpha 7$ -nAChRs, which did not change the IPSCs, including the amplitude of the IPSCs or the direction-selective index (DSI) (Figures 5B and 5C;  $p = 0.36$ ,  $n = 6$ ).

Separately, MLA was applied in the bath solution to block  $\alpha 7$ -nAChRs. Similar to the experiments with HEX, we recorded moving stimuli-evoked IPSCs from On-Off DSGCs (Figure 5D). The application of MLA reduced the IPSCs, both the charge transfer and the DSI (Figures 5E–5G). MLA robustly reduced the IPSCs evoked by stimuli moving in the null direction, but the effect was less for the preferred-direction-evoked IPSCs (Figure 5D). The effect of MLA was later washed out (Figures 5D–5G;  $p = 0.02$  for charge and DSI;  $n = 5$ , repeated-measures ANOVA). These results indicate that MLA-sensitive  $\alpha 7$ -nAChRs in bipolar cells have a role in directional GABA release from SACs, whereas HEX-sensitive non- $\alpha 7$ -nAChRs do not have a significant effect on SACs' direction selectivity.

### **$\alpha 7$ -nAChRs in a subset of bipolar cells contributed to the DSGCs' direction selectivity**

To examine the effect of  $\alpha 7$ -nAChRs in bipolar cells on direction selectivity directly, we used a molecular-biology approach. The ubiquitous  $\alpha 7$ -nAChR knockout mouse model is commercially available; however,  $\alpha 7$ -nAChRs are expressed in many types of retinal neurons that may have roles in direction selectivity (Dmitrieva et al., 2007), making the contributions of  $\alpha 7$ -nAChRs in bipolar cells indistinguishable in that mouse line. Moreover,  $\alpha 7$ -nAChR loss before the developmental stage could lead to unexpected compensation in the retinal circuit. Alternatively, the Cre-loxP technology could enable us to generate a conditional-receptor knockout mouse model (Palazzolo et al., 1990). However, that method is also limited because of the lack of Cre-mouse lines that express Cre-recombinase only in bipolar cells. Therefore, we, instead, used modified Cre technology by the application of Cre-recombinase dependent on green fluorescent protein (Cre-DOG) (Tang et al., 2015). We applied the Cre-DOG technology to a mutant mouse model by crossing the Gus-GFP line, in which, type 7 and a subset of rod bipolar cells express GFP (Wässle et al., 2009), and the *Chrna7-loxP* line, in which, the  $\alpha 7$ -nAChR gene is floxed. To eliminate  $\alpha 7$ -nAChRs from bipolar cells, we injected two kinds of adeno-associated virus (AAV) Cre-DOG viral vectors (see Method details) into the intravitreal space of the mutant mice (Figure S3A).

The effect of Cre-DOG was examined 4 weeks after intraocular injection. For control, we injected saline to Gus-GFP  $\times$  loxP mice and examined  $\alpha 7$ -nAChR-expression by labeling with  $\alpha$ -bungarotoxin-conjugated to Alexa 555; 82% of type-7 bipolar cells colocalized with  $\alpha 7$ -nAChRs (42/51 cells; Figure S3B), which was comparable to our previous data of 89% (Hall et al., 2019). On the other hand, after 4 weeks of Cre-DOG-AAV injection in the mutant mice, only 7 of 87 type-7 bipolar cells colocalized with  $\alpha$ -bungarotoxin ( $n = 7$  mice; Figure S3C). In addition, cre-recombinase generation in GFP-expressing bipolar cells was confirmed by additional intraocular injection with the flex-tdTomato-AAV, in which, bipolar cells partially expressed tdTomato clusters within the dendrites or axons (Figure

S3D). Furthermore, off-target cre-recombinase expression was not detected by the cre-DOG injection because  $\alpha 7$ -nAChR expression in type-2 Off bipolar cells was unaffected (Figure S3E; 47/52 T-2 bipolar cells, 90%,  $n = 3$  mice). These results suggested that  $\alpha 7$ -nAChRs were eliminated solely from type-7 bipolar cells.

Using this mutant mouse model, we recorded from On-Off DSGCs to conduct spike recordings in response to a moving-light stimuli. The identity of recorded On-Off DSGCs was confirmed by immunohistochemistry after the physiological recordings, exhibiting processes co-stratifying with the ChAT bands as well as with somas that were labeled by an antibody against cocaine and amphetamine-regulated transcript (CART) (Figure S4) (Ivanova et al., 2013; Kay et al., 2011).

We first examined whether the IPSCs in mutant DSGCs were reduced compared with those in wild-type (WT) DSGCs, equivalent to the experiment in Figure 5. The On IPSCs evoked by stimuli moving in the null direction were larger than those of preferred-directional stimuli in wild-type mice (Figure 6A; WT) as we also demonstrate in Figure 5. In the mutant-type (MT) mice, the IPSCs were decreased for all directions (Figure 6A; MT). The charge transfer of MT IPSCs was significantly decreased compared with those in WT IPSCs (Figure 6B;  $p < 0.05$ , two-tailed Student's *t* test). Because of the decreased IPSCs, the DSI and the vector sum were unmeasurable. The reduced IPSCs were not due to tissue impairment because IPSCs recordings from non-DSGCs of the mutant mouse did not show the same loss of inhibition (Figure S5;  $n = 5$  ganglion cells,  $p < 0.05$  Student's unpaired *t* test). The results are consistent with the effect of MLA on IPSCs in WT (Figure 5) and indicate a specific role of  $\alpha 7$ -nAChRs in bipolar cells.

Finally, we tested whether  $\alpha 7$ -nAChRs in bipolar cells contribute to direction selectivity in On-Off DSGCs. Because postsynaptic ACh receptors have a role in direction selectivity in On-Off DSGCs at low-contrast light levels (Sethuramanujam et al., 2016), we examined the DSGCs' direction selectivity at various contrast levels. In WT mice, direction selectivity was clearly observed at different levels of moving-stimulus contrast, including 8% and 80% contrast (Figure 6C). Although the average vector sum and DSI at 8% were smaller than for other contrast levels, no significant differences were observed between On and Off responses and among other contrast levels ( $p > 0.1$  in all combinations, Student's *t* test,  $n = 6-8$  DSGCs; Figure 6D). In mutant mice, both the vector sum and DSI of the On spiking responses was significantly decreased compared to WT counterparts ( $p < 0.05$  at 8%, 30%, and 80% contrast;  $n = 7-9$  for 8%, 30%, and 80%;  $n = 4$  for 100% contrast, Student's *t* test; Figures 6E and 6F). In contrast, the Off response DSIs did not significantly decrease compared with that of the WT counterparts. Furthermore, we observed that the number of spikes was increased both for On and Off responses compared with that of WT responses ( $n = 6-7$  DSGCs,  $p < 0.05$ , Student's *t* test; see Discussion for On and Off spikes). Taken together, our results indicate that  $\alpha 7$ -nAChRs in bipolar cells contribute to direction selectivity in On-Off DSGCs.

## DISCUSSION

In this report, we found that bipolar cells receive cholinergic feedback from SACs (Figures 1 and 2), where types-1/2 and type-7 cells expressed  $\alpha 7$ -nAChRs, whereas subsets of type-3 and type-5 bipolar cells expressed non- $\alpha 7$ -nAChRs (Figure 3). Enhanced glutamate release to the SAC proximal dendrites amplifies the signal moving toward the distal dendrites, exceeding the threshold of voltage-gated  $\text{Ca}^{2+}$  channels (Figure 4) and releasing increased GABA to On-Off DSGCs (Figures 5 and 6). Ultimately,  $\alpha 7$ -nAChRs in bipolar cells contribute to On-Off DSGCs' direction-selective spike generation (Figure 6). These findings lead us to propose a model of direction selectivity (Figure 7).

### Mechanisms of direction-selective signaling in On-Off DSGCs and SACs

The existence of retinal ganglion cells sensitive to moving objects has been known for more than 50 years (Barlow and Hill, 1963; Barlow et al., 1964). Two different models for direction selectivity were initially proposed: asymmetric inhibition and excitation. The Barlow-Levick model depends on asymmetric inhibition, in which excitatory inputs to the DSGC initiate spiking in the preferred motion direction, whereas inhibitory inputs veto excitation and silence DSGC spiking in the null direction (Barlow and Levick, 1965). Alternatively, Hassenstein and Reichardt (1956) proposed an asymmetric excitation model, in which two excitatory inputs to the DSGC with distinct delays of signal arrival summate and push the cell over the signaling threshold in the preferred direction, whereas, in the null direction, the two inputs are offset in time, failing to summate and reach the detection threshold.

Subsequent studies have shown that DSGCs are Barlow detectors, receiving excitatory inputs from bipolar cells and SACs via glutamate and ACh, respectively, which is vetoed by asymmetric GABA inhibition from SACs to generate direction-selective signaling (Fried et al., 2002; Taylor and Vaney, 2002; Briggman et al., 2011). Consequently, there is a consensus that GABA input from SACs is required for detection of motion direction in On-Off DSGCs.

SACs also exhibit direction selectivity with enhanced depolarization for objects moving centrifugally from the soma toward the distal dendrites (Euler et al., 2002; Fried et al., 2002). SAC's direction selectivity is considered to be initially produced by spatiotemporal summation along the SAC dendrites and a combination of other mechanisms, such as voltage-gated channels or chloride transporters (Tukker et al., 2004; Enciso et al., 2010; Gavrikov et al., 2006; Hausselt et al., 2007; Oesch and Taylor, 2010; Ozaita et al., 2004). Additionally, lateral inhibition from neighboring SACs enhances direction selectivity, in which centrifugal direction release of GABA from one SAC contributes to the weaker centripetal direction response in the neighboring SAC dendrites (Lee and Zhou, 2006; Zhou and Lee, 2008; Chen et al., 2016; Ding et al., 2016). Finally, excitatory inputs from bipolar cells are restricted to the proximal two-thirds of SAC dendrites, whereas GABA release sites are at the distal dendrites, an arrangement that contributes to direction-selective GABA release (Vlasits et al., 2016; Ding et al., 2016). However, although SACs' direction selectivity appears to use multiple co-operating mechanisms, the contribution of upstream bipolar cells has not been fully understood.

The possibility of bipolar cells' involvement in direction selectivity has been examined. However, multiple studies failed to observe direction-selective responses in individual bipolar cells and, thus, de-emphasized the bipolar cell contribution (Chen et al., 2014; Yonehara et al., 2013; Park et al., 2014). Recent connectomic studies have revealed that SACs receive excitatory synaptic input from multiple bipolar cell types at distinct locations on their dendrites: type-1/2 and type-7 synapse at the SAC proximal dendrites, whereas type 3 and type 5 form synapses at the more-distal dendrites (Ding et al., 2016; Greene et al., 2016; Kim et al., 2014; Helmstaedter et al., 2013). Based on these findings, Kim et al. (2014) proposed a SAC direction-selectivity mechanism, applying the Reichardt asymmetric excitation model to different types of bipolar cells with varying kinetics. However, physiological investigations of this model have not provided a consensus (Fransen and Borghuis, 2017; Stincic et al., 2016; Poleg-Polsky and Diamond, 2016; Matsumoto et al., 2019). However, all these studies are consistent with a contribution of bipolar cells to SAC direction selectivity.

### **Roles of $\alpha 7$ -nAChRs and non- $\alpha 7$ -nAChRs in bipolar cells for retinal direction selectivity**

SACs release ACh in addition to GABA, which is the sole source of ACh in the retina (Famiglietti, 1983; Yan et al., 2020; Hayden et al., 1980). However, the contribution of SAC ACh release to DSGC motion detection has been controversial. Some groups have found that ACh contributes to the direction selectivity of DSGC signaling (Ariel and Daw, 1982; Kittila and Massey, 1997; Sethuramanujam et al., 2016; Lee et al., 2010; Reed et al., 2004), whereas others have found no effect on DSGC motion detection (He and Masland, 1997; Park et al., 2014; Reed et al., 2002). The discrepancy might be attributable to multiple types of nAChRs (IUPHAR/BPS] International Union of Basic and Clinical Pharmacology/British Pharmacological Society, 2020) that were assessed differently among researchers, where some studies used only HEX (blocks  $\alpha 2$ ,  $\alpha 3$ ,  $\alpha 4$ , and  $\alpha 6$  containing nAChRs) but not MLA ( $\alpha 7$ -nAChRs). Additionally, the interpretation of ACh pharmacological results was based on the assumption of postsynaptic nAChR expression in DSGCs but overlooked the contribution of presynaptic nAChRs, including bipolar and amacrine cells (Hall et al., 2019; Dmitrieva et al., 2007). Thus, the contribution of ACh to motion detection remains unclear.

We found that  $\alpha 7$ -nAChRs are expressed by types of bipolar cells that provide inputs to SAC proximal dendrites. In contrast, bipolar cells that provide inputs at more-distal dendrites either did not express nAChRs or expressed non- $\alpha 7$ -nAChRs (Figures 3 and 7). Throughout the brain, presynaptic expression of either  $\alpha 7$ -nAChRs or non- $\alpha 7$ -nAChRs facilitates the release of neurotransmitters, such as glutamate (McGehee et al., 1995; Gray et al., 1996; Alkondon et al., 1996). This occurs through either membrane depolarization or increased conductance of calcium to evoke transmitter release (Léna et al., 1993; Wonnacott et al., 2006; Mulle et al., 1992; Vernino et al., 1992).  $\alpha 7$ -nAChRs are especially distinguished by their high calcium permeability, which is several orders of magnitude greater than that for non- $\alpha 7$ -nAChRs (Haghighi and Cooper, 2000; Bertrand et al., 1993; Séguéla et al., 1993; Alkondon et al., 1996; Fucile, 2004).

In our recordings from bipolar cells, we did not observe significant differences in the amplitude or kinetics of EPSCs mediated by  $\alpha 7$ -nAChRs and non- $\alpha 7$ -nAChRs (Figure

3). In general, synaptic transmission via both  $\alpha 7$ -nAChRs and non- $\alpha 7$ -nAChRs occurs on the order of a few milliseconds (Stanchev and Sargent, 2011; Lamotte d'Incamps et al., 2008), and  $\alpha 7$ -nAChRs are known for fast rise times and rapid desensitization compared with other nAChR types (Albuquerque et al., 2009). The discrepancy between the general consensus and our bipolar cell results may be related to certain factors. SACs are considered to use volume transmission of ACh (Brombas et al., 2017; Sethuramanujam et al., 2016), which could lead to delayed opening of individual nicotinic channels. In addition, the cable properties of thin bipolar cell axons might alter the observed kinetics because nAChRs were stimulated at the axon terminal but were recorded at the soma. Finally, heteromeric  $\alpha 7\beta 2$ -nAChRs, rather than homomeric  $\alpha 7$ -nAChRs, could mediate MLA-sensitive EPSCs in bipolar cells because they exhibit similar MLA-sensitivity but slower signaling kinetics (Khiroug et al., 2002). Regardless, the high calcium permeability of  $\alpha 7$ -nAChRs suggests cholinergic feedback to  $\alpha 7$ -expressing bipolar cell types would result in enhanced release of glutamate to postsynaptic neurons relative to other bipolar cell types.

All these reports and our results suggest that cholinergic feedback from SACs to bipolar cells that provide synaptic input restricted to the central portion of SAC dendrites produces a greater excitation than those at the more distal dendrites. Therefore, we propose that the boosted excitation to the central part of SAC dendrites has a role in generating their centrifugal direction selectivity for motion from the SAC soma toward the distal dendrites (Figure 7).

Furthermore, the relation between stimulus contrast and the contribution of nAChRs has been previously investigated. Poleg-Polsky and Diamond (2016) demonstrated that On-Off DSGCs must balance the amount of excitation and inhibition at different levels of stimulus contrast to maintain correct direction-selective signaling under varying stimulus conditions. To maintain that balance, they suggested that excitatory glutamate inputs to On-Off DSGCs were mediated by specific bipolar cell types, whereas a separate set of bipolar cells drive feedforward inhibition via GABA release from SACs. Furthermore, Sethuramanujam et al. (2016) reported that DSGC EPSCs for low-contrast moving stimuli were mediated by the coordination of postsynaptic depolarization by HEX-sensitive nAChRs and NMDA receptors (see also Sethuramanujam et al. [2017]). In light of those seminal works, we examined the effect of presynaptic nAChRs on DSGC spike generation by stimulating the retina with moving bars of various contrast levels (Figure 6). We found that  $\alpha 7$ -nAChRs in distinct bipolar cell types enhanced GABA release from SACs to On-Off DSGCs (Figure 5), and genetic elimination of type-7 bipolar cell  $\alpha 7$ -nAChRs led to reduced direction selectivity of DSGCs at 8%, 30%, and 80% contrast, relative to that of WT mice (Figure 6). Because connectomic studies indicate that  $\alpha 7$ -expressing types-1, -2, and -7 bipolar cells provide minimal input to On-Off DSGCs (Helmstaedter et al., 2013), presynaptic  $\alpha 7$ -nAChRs in these bipolar cells likely contribute to GABA release from SACs to On-Off DSGCs across different contrast levels. Alternatively, HEX-sensitive nAChRs in type-3 and type-5 bipolar cells did not contribute to GABA release from SACs. However, these bipolar cell types provide most direct glutamate inputs to On-Off DSGCs (Helmstaedter et al., 2013), suggesting that future studies will be required to determine the contribution of HEX-sensitive non- $\alpha 7$ -nAChRs at pre- or postsynaptic sites under different contrast conditions.

### **$\alpha$ 7-nAChRs in bipolar cells as a contributing factor for SACs' direction selectivity**

Our data of SAC computational analysis and ganglion cell recordings show that nAChRs in bipolar cells are a crucial component of DSGC motion detection. It has been a consensus that GABA inhibition, both between neighbor SACs and from wide-field amacrine cells, is important factors for SACs' direction selectivity (Lee and Zhou, 2006; Pei et al., 2015; Huang et al., 2019). However, adding nAChRs in bipolar cells boosted the direction selectivity in SAC dendrites (Figure 4). Along with mechanisms that include the GABA inhibitory system (Lee and Zhou, 2006; Pei et al., 2015), the structure of SAC inputs/outputs (Vlasits et al., 2016), and others,  $\alpha$ 7-nAChRs in bipolar cells are an essential factor for SACs' direction selectivity. Our work also sheds light on the role of bipolar cells and ACh in direction selective mechanisms, which has been controversial. Although our findings suggest that cholinergic feedback to nAChRs in bipolar cells contributes to motion detection under low-contrast conditions, other functions may also arise from this feedback as well. Although we did not explore the possibility here, presynaptic nAChRs could also enhance motion detection when the moving object is covered by other objects in the visual field, such as a bird flying behind a tree. Because SAC distal dendrite transmitter release is known to precede the moving object itself for lateral motion (Koren et al., 2017), leading cholinergic inputs by neighbor SACs to bipolar cells could facilitate motion detection even if some bipolar cell inputs were absent because of the obstructive objects. Future studies may clarify how the coordination of many distinct mechanisms facilitates motion detection in the retina. These factors should complement each other to encode object motion that occurs in various forms in the visual world, such as at different speeds and contrasts and in changing ambient light conditions.

#### **Limitations of the study**

Our computational modeling shows that presynaptic nAChRs boost SAC's voltage and calcium signaling in response to centrifugally moving stimuli (Figure 4). However, there were some limitations for the simulation parameters. First, the ACh release sites in SAC dendrites have not been fully elucidated. We placed the ACh release site at the SAC distal dendrites along with the GABA release site based on the observations that SACs' input and output distribution is polarized (Famiglietti, 1991; Vlasits et al., 2016). Second, SAC dendrites are functionally compartmentalized to prevent signal spread from one branch to others (Koren et al., 2017), which may occur by GABA receptors (Poleg-Polsky et al., 2018), mGluR2 (Koren et al., 2017), or Kv3 channels (Ozaita et al., 2004). In our model, Kv3 channels and GABA receptors were located in the proximal dendrites (Ding et al., 2016). Third, the model included only one type of nicotinic receptor without any possible differences in its physiological properties (Figure 4).

In addition, after knocking out  $\alpha$ 7-nAChRs from type-7 bipolar cells, we found that On-Off DSGCs in the mutant retina exhibited increased spiking for both null- and preferred-direction motion for both ON and OFF responses (Figure 6), despite the specificity of the Cre-DOG for GFP-expressing type-7 On bipolar cells (Figures S2 and S3E). This suggests that although Off and On SACs are geographically separated in the retina, some cross-talk between these pathways may exist downstream. One such possible cross-talk could occur through the understudied DAPI-3 amacrine cell, a glycinergic amacrine cell that

is bistratified near the level of the On and Off ChAT bands (Wright et al., 1997; Zucker et al., 2005). Alternatively, it might be explained by a fact that On- or Off-stratifying dendrites of On-Off DSGCs frequently cross over into the opposing sublaminae upstream of the soma (Huang et al., 2021).

## STAR★METHODS

### RESOURCE AVAILABILITY

**Lead contact**—Further information and requests for resources and reagents should be directed to and will be fulfilled by the lead contact, Tomomi Ichinose (tichinos@med.wayne.edu).

**Materials availability**—Mice strains and viral vectors generated in this study will be made available on request, but we may require a payment and/or a completed Materials Transfer Agreement if there is potential for commercial application.

### Data and code availability

- The dataset generated by the electrophysiological experiments and immunohistochemistry in this paper is available on request from the lead contact.
- The scripts and data for Figure 4 are in the subfolder nc/models/sbac\_nrecep. The Neuron-C package compiles and runs under Linux and Mac OSX.
- Any additional information required to reanalyze the data reported in this paper is available from the lead contact upon request.

### EXPERIMENTAL MODEL AND SUBJECT DETAILS

**Animals**—Experiments were performed using healthy adult mice (4–12 weeks old, male or female) including from C57BL/6J (RRID: IMSR\_JAX:000664) mice. For optogenetic experiments, Chat-IRES-Cre mice (RRID: IMSR\_JAX:031661) were crossed with Ai32-ChR2-YFP mice (RRID: IMSR\_JAX:024109). For  $\alpha 7$ -nAChR knockout mice, Gus8.4-GFP mice (RRID: IMSR\_JAX:026704) were crossed with  $\alpha 7$ -nAChR-FLOX mice (RRID: IMSR\_JAX:026965). Animals were housed in 12-hour light-dark cycles, in groups up to 5 animals per cage. All animal procedures were approved by the Institutional Animal Care and Use Committee at Wayne State University (protocol no. 17–11-0399). All the necessary steps were taken to minimize animal suffering. The tissues were harvested immediately after the animal was euthanized by CO<sub>2</sub> inhalation and cervical dislocation.

### METHOD DETAILS

**Retinal preparation**—The experimental techniques were similar to previously described ((Ichinose and Lukasiewicz, 2012); Ichinose et al., 2014). Briefly, mice were dark-adapted at least one hour prior to dissection. The eyes were enucleated and the retina was isolated and cut into flat-mount preparations. For immunohistochemistry, retinal slices were also prepared where the retina was placed on a piece of filter membrane (HABG01300, Millipore-Sigma, Burlington, MA) and cut into slice preparations (250  $\mu$ m thick) using a hand-made chopper (Hellmer and Ichinose, 2015). All procedures were performed in

dark-adapted conditions under infrared illumination using infrared viewers. The dissecting medium was cooled and continuously oxygenated. Retinal preparations were stored in an oxygenated dark box at room temperature.

**Whole-cell recordings**—Whole-cell patch clamp recordings were made from the bipolar cell, ON-SAC, and ON-OFF DSGC somas in wholemount retinal preparations by viewing them with an upright microscope (Slicescope Pro 2000, Scientifica, UK) equipped with a CCD camera (Retiga-2000R, Q-Imaging, Surrey, Canada). Tissues were immobilized using a platinum horseshoe net with nylon wires over the tissue. The light-evoked postsynaptic potentials and currents (L-EPSPs and L-EPSCs) were recorded at the resting membrane potential for current clamp, or at  $-55\text{mV}$  for voltage clamp recordings, near the equilibrium potential for chloride. All recordings were performed at  $30\text{--}34^\circ\text{C}$ . Whole-cell recordings from bipolar cells lasted as long as 20–30 minutes without significant rundown (Ichinose et al., 2014). The electrodes were pulled from borosilicate glass (1B150F-4; WPI, Sarasota, FL) with a P1000 Puller (Sutter Instruments, Novato, CA) and had resistances of 5–7 M $\Omega$  for ganglion cell recordings and 8–12 M $\Omega$  for bipolar cell recordings. Clampex and MultiClamp 700B (Molecular Devices, San Jose, CA) were used to generate the waveforms, acquire the data, and control light stimuli by a light-emitting diode (LED) (Cool LED, Andover, UK). The data were digitized and stored on a personal computer using Axon Digidata 1440A (Molecular Devices). The responses were filtered at 1 kHz with the four-pole Bessel filter on the MultiClamp 700B and sampled at 2–5 kHz.

Bipolar cells and DSGCs were blindly targeted. In the wholemount retinal tissue, pipettes were advanced deeply into the tissue from ganglion cell side until the outer half of the inner nuclear layer (50–80 $\mu\text{m}$  from the tissue surface). Then, whole cell configuration was made from a soma and light response were recorded. The type of bipolar cells was morphologically determined (see Figure S2 for detail). For ganglion cell recordings, relatively large and ovular somas were targeted and whole cell configuration was made. Recordings from ON and OFF DSGCs was confirmed if they exhibited both onset and offset spikes and/or EPSPs in response to a step light stimulus and direction selectivity with the DSI higher than 0.3 (Pei et al., 2015; Jacoby and Schwartz, 2017). Alternatively, the cell was labeled with Neurobiotin and post-fixation staining with the anti-CART antibody (H003–62, Phoenix Pharmaceuticals, Inc. Burlingame, CA), which labels ON and OFF DSGCs (Kay et al., 2011) to verify DSGCs from the Gus-GFP and loxP mice,

**Solutions and drugs**—The retinal dissections were performed in HEPES-buffered extracellular solution containing the following (in mM): 115 NaCl, 2.5 KCl, 2.5 CaCl<sub>2</sub>, 1.0 MgCl<sub>2</sub>, 10 HEPES, and 28 glucose, adjusted to pH 7.37 with NaOH. Physiological recordings were performed in Ames' medium buffered with NaHCO<sub>3</sub> (Millipore-Sigma) and bubbled with 95% O<sub>2</sub> and 5% CO<sub>2</sub>; the pH was 7.4 at 30 – 33°C. The intracellular solution contained the following (in mM): 110 potassium methanesulfonate, 10 HEPES, 4 EGTA, 5 NaCl, 5 KCl, 1 MgCl<sub>2</sub>, 4 ATP-Mg, and 1 GTP-Na, adjusted to pH 7.2 with KOH. For voltage-clamp recordings, the intracellular solution contained the following: 110 cesium methanesulfonate, 10 HEPES, 10 TEA-Cl, 4 EGTA, 1 MgCl<sub>2</sub>, 5 mM QX-314, 4 ATP-Mg, and 1 GTP-Na, adjusted to pH 7.2 with CsOH. To block photoreceptor inputs to bipolar

cells and SACs, 10 mM L-AP4 (Tocris), 1  $\mu$ M ACET (Tocris), and 50  $\mu$ M GYKI53655 (Tocris, Bristol, UK) were perfused in the bath solution. To block nAChR currents, 100nM methyllycaconitine citrate (MLA, Tocris) or 100  $\mu$ M hexamethonium (HEX, Tocris) were perfused in addition to the photoreceptor blockers. Either MLA or HEX was applied first in random order, and subsequently the combination of both antagonists was perfused to block nAChR currents. Retinal photoreceptor blockers were perfused for 5–15 minutes, and then each nAChR antagonist was perfused for 5–15 minutes during recordings.

**Light stimulation**—Retinal wholemount tissues were light-adapted at  $1 \times 10^5$  photons/ $\mu\text{m}^2/\text{s}$  in the recording chamber. Bipolar cells were initially presented with a 1 s step light (500nm, 20% Weber contrast,  $1 \times 10^7$  photons/ $\mu\text{m}^2/\text{s}$ , 150 $\mu\text{m}$  diameter). Then, photoreceptor input was blocked with 1 $\mu$ M ACET (kainite receptor) + 10 $\mu$ M L-AP4 (mGluR6) + 50 $\mu$ M GYKI53655 (AMPA), and the light response was recorded every 30 s until it disappeared. After, a 1 s step light (500nm,  $1 \times 10^{10}$  photons/ $\mu\text{m}^2/\text{s}$ , 150 $\mu\text{m}$  diameter) was used to optogenetically depolarize ON and OFF-SACs. ChR2 was optogenetically activated using the 500nm light instead of 470nm light, which still allows for ~80% of the peak ChR2 conductance (Nagel et al., 2003). To confirm that photoreceptor inputs did not remain when using the higher step light intensity for ChR2, we also presented a 565nm step light at  $1 \times 10^{10}$  photons/ $\mu\text{m}^2/\text{s}$  after photoreceptors were pharmacologically blocked, which is outside the absorption spectrum for ChR2 (Nagel et al., 2003).

For DSGCs, after the patch clamp configuration was made, the objective lens was switched to a 10x, and green light (wavelength 500 nm) with different patterns was presented through the objective (Polygon). A step of light with a circular shape (diameter 500 $\mu\text{m}$ ) was presented to examine whether the cell was an ON-OFF responding ganglion cell. The moving light stimulus was constructed using a longitudinal bar of 600  $\mu\text{m}$  (width) and 160  $\mu\text{m}$  (height). The bar moved from 150  $\mu\text{m}$  away from the soma in 8 directions at a speed of 600  $\mu\text{m}/\text{s}$ , which separated the ON and OFF responses by approximately 1 s. The contrast of the light stimulus was 8, 30, and 80% (Weber contrast).

**Morphological identification of bipolar cells**—A fluorescent dye, sulforhodamine B (0.005%, Millipore-Sigma) was included in the patch clamp pipette. Immediately after electrophysiological recordings, sulforhodamine B images were captured using the CCD camera. As the ON and OFF ChAT bands are labeled with EYFP in Ai32  $\times$  ChAT-Cre mice, we used these as reference points for axon terminal depth in the IPL. We determined bipolar cell types according to previous descriptions (Ghosh et al., 2004; Ichinose et al., 2014; Ichinose and Hellmer, 2016). Briefly, each type was determined as follows: Type 1/2: below or in focus to OFF ChAT, Type 3: inner to OFF ChAT, Type 4: outer 1/3 of the IPL, Type 5: outer to or in focus to ON ChAT, Type 6: inner to ON ChAT but extend vertically to the ganglion cell layer, Type 7: inner to ON ChAT but extend laterally parallel to ChAT band. However, because we relied on morphology alone to identify bipolar cells types, type 1 and 2, 3a and 3b, and subsets of type 5 bipolar cells could not be individually distinguished.

**Immunohistochemistry**—Retinal slice sections or wholemount sections were used for immunohistochemistry. For  $\alpha$ -bungarotoxin staining, we used live retinal slice sections and  $\alpha$ -bungarotoxin conjugated to Alexa 555 (1:100, Thermofisher, Waltham, MA) was applied

for 1 hour, followed by several rinses with HEPES buffer solution prior to fixation. For type-2 bipolar cells were labeled with the synaptotagmin 2 antibody (Zebrafish International Research Center, OR). For the model SAC morphology, a tdTomato labeled SAC was filled with Neurobiotin tracer (0.5%, Vector Lab, Burlingame, CA) for 60 minutes in the wholemount retina prior to fixation. Slice or wholemount sections were fixed for 30 or 60 minutes, respectively, in 4% paraformaldehyde (PFA) in 0.1M phosphate buffer (PB) solution. Sections were subsequently washed three times for 15 minutes each in 0.1M PB solution, and then blocked with 10% normal donkey serum (NDS) in 0.01M phosphate buffered saline with 0.5% Triton-X (PBS-T) for 1 hour at room temperature. Primary antibodies were dissolved in 3% PBS-T and applied overnight at room temperature, and then incubated with secondary antibodies for 2 hours at room temperature. Preparations were viewed with a confocal microscope (TCS SP8, Leica, Wetzlar, Germany) using a variety of objectives. Neurobiotin or ChR2-YFP labeled SACs were viewed using a 40 × water immersion objective lens with a z-step of 0.5μm, while α-bungarotoxin labeled slices were viewed using a 63 × water immersion objective using a z-step of 0.3μm. For double-labeled tissues, sequential scanning was used to eliminate crosstalk between channels.

**AAV application**—We utilized two AAV viral vectors that contain the DNA constructs of N and C-terminal Cre-DOG plasmids (plasmid #69572 and #69573, AddGene, Cambridge, MA), and WPRE and polyA sites were added into the plasmid sequences. The flex-tdTomato-AAV was generated with the plasmid (#28306, AddGene). The AAV vectors were packaged and affinity purified by Virovek (Hayward, CA, USA). The serotype of the AAV was the AAV2.7m8, which enables retinal interneuron transfection (Byrne et al., 2014). We injected the viral vectors into the intravitreal space of Gus-GFP × α7-nAChR<sup>flox</sup> mouse eyes at a concentration of  $\sim 1 \times 10^{11}$  vg/mL using the Nanoject III (Drummond, Broomall, PA). After 4 weeks post-injection, we expected to observe that the GFP-expressing type 7 bipolar cells develop the Cre-recombinase, eliminating the floxed α7-nAChRs without affecting other no-GFP neurons (Figure S2).

**Modeling**—We constructed a model of 3 mouse SACs and their bipolar cell inputs using the simulation language Neuron-C (Smith, 1992). We digitized a mouse SAC morphology from an image of a cell injected with fluorescent dye, noting the most distal dendritic regions, 70–150 μm from the soma, where presynaptic varicosities were located. To capture the dendritic electrotonic decay, we included a multiplicative “diameter factor” based on least-squares fits of capacitive charging from a somatic voltage pulse in previous studies (Stincic et al., 2016). The dendrites of each SAC were discretized into compartments of 0.02 space constant, producing a model of each SAC containing 657 compartments. We chose biophysical parameters ( $V_{rest}$  70 mV,  $R_i$  100 Ohm-cm,  $R_m$  50,000 Ohm-cm<sup>2</sup>) for the SAC model based on previous studies (Stincic et al., 2016; Chen et al., 2020; Ding et al., 2016). Synapses were modeled as Ca<sup>2+</sup>-driven neurotransmitter release that bound to a postsynaptic channel defined by a ligand-activated Markov sequential-state machine (Smith, 1992). Membrane ion channels were defined by a voltage-gated Markov state machine and were placed at densities specified for each region of the cell. Voltage-gated potassium and calcium channels were included in SAC dendrites at densities consistent with previous studies (Ozaita et al., 2004; Koren et al., 2017). See Table S2 for biophysical parameters.

Bipolar cells were generated in a semi-random pattern and synaptically connected to SAC dendrites within a criterion distance (typically 10–15  $\mu\text{m}$ ). Bipolar cell synapses contacted the SAC dendritic tree within 70–90  $\mu\text{m}$  of the SAC soma, but were excluded from the more distal region of synaptic varicosities based on the original cell image and the spacing and distribution patterns of bipolar cell inputs onto SACs reported in connectomic analysis (Ding et al., 2016; Greene et al., 2016). Bipolar cells were given a simple artificial morphology, with a soma and an axon connected to a presynaptic terminal where synapses were made onto the SACs.

The 3-SAC network was assembled with an algorithm that synaptically interconnected the SAC dendrites based on their location and orientation. The SAC spacing (65  $\mu\text{m}$ ) was set so that their distal dendrites (70–100  $\mu\text{m}$  from the soma) made inhibitory synapses onto their SAC neighbors within 40  $\mu\text{m}$  of the neighbor somas. Each SAC typically made a total of 45–60 inhibitory synapses onto its nearest neighbor(s). The central SAC received about 50% more inhibitory synapses than the surrounding SACs because it had 2 neighbors: the “edge effect.” Therefore, to achieve a balance between inhibition in the central SAC and its 2 surrounding SACs, we increased the conductance of the central- > surround inhibitory synapses by 50%.

Stimuli were presented to the SAC model by voltage-clamping the bipolar cell somas according to the stimulus spatiotemporal pattern. The stimulus contrast was defined as a voltage increment depolarizing the soma from the background holding potential, which was set just above the threshold for synaptic release, typically  $-50$  to  $-45$  mV. The bipolar cell synapses had an exponential release function with a gain of 3 mV/e-fold change, and each had a conductance that varied between 10 and 50 pS. This set the strength of excitatory output from bipolar cells to the SACs.

In some model runs, we included cholinergic feedback to bipolar cells. As release of ACh is thought to occur exclusively from the distal region of varicosities, which does not receive bipolar synaptic contacts, the cholinergic feedback was only transmitted to bipolar cells that made contact with neighboring SAC(s). To simulate this cholinergic feedback, we included excitatory synapses (50–100 pS) from the most distal SAC dendrites onto the axon terminals of bipolar cells. By virtue of their distal location ( $> 100$   $\mu\text{m}$  from the soma) and the cell spacing (65  $\mu\text{m}$ ) these synapses were excluded from contacting bipolar cells within the neighbor SAC’s zone of proximal inhibition, and thus contacted bipolar cells  $\sim 35$ –80  $\mu\text{m}$  from the neighbor SAC somas.

Models were run on an array of 3.2 GHz AMD Opteron CPUs interconnected by Gigabit ethernet, on the Mosix parallel distributed task system under the Linux operating system.

## QUANTIFICATION AND STATISTICAL ANALYSIS

The charge transfer was measured for the IPSCs. The number of spikes was counted for loose patch recordings. The direction-selective index (DSI) was calculated as follows:

Along with DSI, we generated a vector sum of the magnitude of responses where the sum is equal to (1 - Direct Circular Variance) (Mazurek et al., 2014; Taylor and Vaney, 2002).

All values are presented as the mean  $\pm$  SEM. Some bipolar cells with ChR2-evoked currents (ChR2-EPSCs) did not have complete sets of pharmacology but were still included for analysis (i.e., Control versus Drug 1 versus Drug 1+2). Therefore, a mixed-model ANOVA was used to compare the ChR2-EPSCs before and after the application of multiple nAChR antagonist combinations (Prism v.8, GraphPad Software, San Diego, CA). The mixed-model ANOVA was run with a Geisser-Greenhouse correction to account for possible violations of the assumption of circularity/sphericity, followed by a Tukey's multiple comparisons test to obtain the adjusted *p-values*. A paired t test was used to compare the light response of bipolar cells before and after application of glutamate antagonists. For ooDSGCs, IPSCs were compared using paired Students-tests (Figure 5), while ON and OFF spiking for different contrast levels were analyzed using unpaired Students t tests between WT and MT conditions (Figure 6). The differences were considered significant if  $p < 0.05$ .

## Supplementary Material

Refer to Web version on PubMed Central for supplementary material.

## ACKNOWLEDGMENTS

Authors are grateful to Ms. C. Koehler for her technical assistance. This study was supported by NIH EY028915 and EY032917 and Research to Prevent Blindness (RPB) grants to T.I., NIH EY022070 to R.G.S., the Interdisciplinary Biomedical Sciences (IBS) and Rumble Fellowship to C.B.H., RPB Medical Student Fellowship to L.M.H., and the IBS Fellowship to J.M.B.

## REFERENCES

- Albuquerque EX, Pereira EF, Alkondon M, and Rogers SW (2009). Mammalian nicotinic acetylcholine receptors: from structure to function. *Physiol. Rev.* 89, 73–120. [PubMed: 19126755]
- Alkondon M, and Albuquerque EX (1993). Diversity of nicotinic acetylcholine receptors in rat hippocampal neurons. I. Pharmacological and functional evidence for distinct structural subtypes. *J. Pharmacol. Exp. Ther.* 265, 1455–1473. [PubMed: 8510022]
- Alkondon M, Rocha ES, Maelicke A, and Albuquerque EX (1996). Diversity of nicotinic acetylcholine receptors in rat brain. V. alpha-Bungarotoxin-sensitive nicotinic receptors in olfactory bulb neurons and presynaptic modulation of glutamate release. *J. Pharmacol. Exp. Ther.* 278, 1460–1471. [PubMed: 8819534]
- Ariel M, and Daw NW (1982). Pharmacological analysis of directionally sensitive rabbit retinal ganglion cells. *J. Physiol.* 324, 161–185. [PubMed: 7097594]
- Barlow HB, and Hill RM (1963). Selective sensitivity to direction of movement in ganglion cells of the rabbit retina. *Science* 139, 412–414. [PubMed: 13966712]
- Barlow HB, and Levick WR (1965). The mechanism of directionally selective units in rabbit's retina. *J. Physiol.* 178, 477–504. [PubMed: 5827909]
- Barlow HB, Hill RM, and Levick WR (1964). Retinal ganglion cells responding selectively to direction and speed of image motion in the rabbit. *J. Physiol.* 173, 377–407. [PubMed: 14220259]
- Bertrand D, Galzi JL, Devillers-Thiéry A, Bertrand S, and Changeux JP (1993). Mutations at two distinct sites within the channel domain M2 alter calcium permeability of neuronal alpha 7 nicotinic receptor. *Proc. Natl. Acad. Sci. USA* 90, 6971–6975. [PubMed: 7688468]
- Briggman KL, Helmstaedter M, and Denk W (2011). Wiring specificity in the direction-selectivity circuit of the retina. *Nature* 471, 183–188. [PubMed: 21390125]
- Brombas A, Kalita-de Croft S., Cooper-Williams EJ, and Williams SR (2017). Dendro-dendritic cholinergic excitation controls dendritic spike initiation in retinal ganglion cells. *Nat. Commun.* 8, 15683. [PubMed: 28589928]

- Byrne LC, Oztürk BE, Lee T, Fortuny C, Visel M, Dalkara D, Schaffer DV, and Flannery JG (2014). Retinoschisin gene therapy in photoreceptors, Müller glia or all retinal cells in the *Rs1h*<sup>-/-</sup> mouse. *Gene Ther.* 21, 585–592. [PubMed: 24694538]
- Chen M, Lee S, Park SJ, Looger LL, and Zhou ZJ (2014). Receptive field properties of bipolar cell axon terminals in direction-selective sublaminae of the mouse retina. *J. Neurophysiol.* 112, 1950–1962. [PubMed: 25031256]
- Chen Q, Pei Z, Koren D, and Wei W (2016). Stimulus-dependent recruitment of lateral inhibition underlies retinal direction selectivity. *eLife* 5, e21053. [PubMed: 27929372]
- Chen Q, Smith RG, Huang X, and Wei W (2020). Preserving inhibition with a disinhibitory microcircuit in the retina. *eLife* 9, e62618. [PubMed: 33269700]
- Ding H, Smith RG, Poleg-Polsky A, Diamond JS, and Briggman KL (2016). Species-specific wiring for direction selectivity in the mammalian retina. *Nature* 535, 105–110. [PubMed: 27350241]
- Dmitrieva NA, Strang CE, and Keyser KT (2007). Expression of alpha 7 nicotinic acetylcholine receptors by bipolar, amacrine, and ganglion cells of the rabbit retina. *J. Histochem. Cytochem.* 55, 461–476. [PubMed: 17189521]
- Enciso GA, Rempe M, Dmitriev AV, Gavrikov KE, Terman D, and Mangel SC (2010). A model of direction selectivity in the starburst amacrine cell network. *J. Comput. Neurosci.* 28, 567–578. [PubMed: 20524107]
- Euler T, Detwiler PB, and Denk W (2002). Directionally selective calcium signals in dendrites of starburst amacrine cells. *Nature* 418, 845–852. [PubMed: 12192402]
- Famiglietti EV Jr. (1983). ‘Starburst’ amacrine cells and cholinergic neurons: Mirror-symmetric on and off amacrine cells of rabbit retina. *Brain Res.* 261, 138–144. [PubMed: 6301622]
- Famiglietti EV (1991). Synaptic organization of starburst amacrine cells in rabbit retina: analysis of serial thin sections by electron microscopy and graphic reconstruction. *J. Comp. Neurol.* 309, 40–70. [PubMed: 1894768]
- Fransen JW, and Borghuis BG (2017). Temporally diverse excitation generates direction-selective responses in on- and off-type retinal starburst amacrine cells. *Cell Rep.* 18, 1356–1365. [PubMed: 28178515]
- Fried SI, Münch TA, and Werblin FS (2002). Mechanisms and circuitry underlying directional selectivity in the retina. *Nature* 420, 411–414. [PubMed: 12459782]
- Fucile S (2004). Ca<sup>2+</sup> permeability of nicotinic acetylcholine receptors. *Cell Calcium* 35, 1–8. [PubMed: 14670366]
- Fyk-Kolodziej B, and Pourcho RG (2007). Differential distribution of hyperpolarization-activated and cyclic nucleotide-gated channels in cone bipolar cells of the rat retina. *J. Comp. Neurol.* 501, 891–903. [PubMed: 17311321]
- Gavrikov KE., Nilson JE., Dmitriev AV., Zucker CL., and Mangel SC. (2006). Dendritic compartmentalization of chloride cotransporters underlies directional responses of starburst amacrine cells in retina. *Proc. Natl. Acad. Sci. USA* 103, 18793–18798. [PubMed: 17124178]
- Ghosh KK, Bujan S, Haverkamp S, Feigenspan A, and Wässle H (2004). Types of bipolar cells in the mouse retina. *J. Comp. Neurol.* 469, 70–82. [PubMed: 14689473]
- Gray R, Rajan AS, Radcliffe KA, Yakehiro M, and Dani JA (1996). Hippocampal synaptic transmission enhanced by low concentrations of nicotine. *Nature* 383, 713–716. [PubMed: 8878480]
- Greene MJ, Kim JS, and Seung HS; EyeWriters (2016). Analogous convergence of sustained and transient inputs in parallel on and off pathways for retinal motion computation. *Cell Rep.* 14, 1892–1900. [PubMed: 26904938]
- Haghighi AP, and Cooper E (2000). A molecular link between inward rectification and calcium permeability of neuronal nicotinic acetylcholine  $\alpha 3\beta 4$  and  $\alpha 4\beta 2$  receptors. *J. Neurosci.* 20, 529–541. [PubMed: 10632582]
- Hall LM, Hellmer CB, Koehler CC, and Ichinose T (2019). Bipolar cell type-specific expression and conductance of alpha-7 nicotinic acetylcholine receptors in the mouse retina. *Invest. Ophthalmol. Vis. Sci.* 60, 1353–1361. [PubMed: 30934054]

- Hassenstein V, and Reichardt W (1956). System theoretical analysis of time, sequence, and sign analysis of the motion perception of the snout-beetle *Chlorophanus*. *Z. Naturforsch. B* 11, 513–524.
- Hausselt SE, Euler T, Detwiler PB, and Denk W (2007). A dendrite-autonomous mechanism for direction selectivity in retinal starburst amacrine cells. *PLoS Biol.* 5, e185. [PubMed: 17622194]
- Hayden SA, Mills JW, and Masland RM (1980). Acetylcholine synthesis by displaced amacrine cells. *Science* 210, 435–437. [PubMed: 7433984]
- He S, and Masland RH (1997). Retinal direction selectivity after targeted laser ablation of starburst amacrine cells. *Nature* 389, 378–382. [PubMed: 9311778]
- Hellmer CB, and Ichinose T (2015). Recording light-evoked postsynaptic responses in neuron in dark-adapted, mouse retinal slice preparations using patch clamp techniques. *J. Vis. Exp.* 96.
- Hellmer CB, Zhou Y, Fyk-Kolodziej B, Hu Z, and Ichinose T (2016). Morphological and physiological analysis of type-5 and other bipolar cells in the mouse retina. *Neuroscience* 315, 246–258. [PubMed: 26704635]
- Helmstaedter M, Briggman KL, Turaga SC, Jain V, Seung HS, and Denk W (2013). Connectomic reconstruction of the inner plexiform layer in the mouse retina. *Nature* 500, 168–174. [PubMed: 23925239]
- Huang X, Rangel M, Briggman KL, and Wei W (2019). Neural mechanisms of contextual modulation in the retinal direction selective circuit. *Nat. Commun.* 10, 2431. [PubMed: 31160566]
- Huang X, Kim AJ, Ledesma HA, Ding J, Smith RG, and Wei W (2021). Visual stimulation induces distinct forms of sensitization of On-Off direction-selective ganglion cell responses in the dorsal and ventral retina. *bioRxiv.* 10.1101/2019.12.19.873364.
- Ichinose T, and Hellmer CB (2016). Differential signalling and glutamate receptor compositions in the OFF bipolar cell types in the mouse retina. *J. Physiol.* 594, 883–894. [PubMed: 26553530]
- Ichinose T, Fyk-Kolodziej B, and Cohn J (2014). Roles of ON cone bipolar cell subtypes in temporal coding in the mouse retina. *J. Neurosci.* 34, 8761–8771. [PubMed: 24966376]
- Ichinose T, and Lukasiewicz PD (2012). The mode of retinal presynaptic inhibition switches with light intensity. *J. Neurosci.* 32, 4360–4371. [PubMed: 22457487]
- [IUPHAR/BPS] International Union of Basic and Clinical Pharmacology/British Pharmacological Society (2020). *Guide to Pharmacology.*
- Ivanova E, Lee P, and Pan ZH (2013). Characterization of multiple bistratified retinal ganglion cells in a purkinje cell protein 2-Cre transgenic mouse line. *J. Comp. Neurol.* 521, 2165–2180. [PubMed: 23224947]
- Jacoby J, and Schwartz GW (2017). Three small-receptive-field ganglion cells in the mouse retina are distinctly tuned to size, speed, and object motion. *J. Neurosci.* 37, 610–625. [PubMed: 28100743]
- Kay JN, De La Huerta I, Kim I-J, Zhang Y, Yamagata M, Chu MW, Meister M, and Sanes JR (2011). Retinal ganglion cells with distinct directional preferences differ in molecular identity, structure, and central projections. *J. Neurosci.* 31, 7753–7762. [PubMed: 21613488]
- Khiroug SS, Harkness PC, Lamb PW, Sudweeks SN, Khiroug L, Millar NS, and Yakel JL (2002). Rat nicotinic ACh receptor  $\alpha 7$  and  $\beta 2$  subunits co-assemble to form functional heteromeric nicotinic receptor channels. *J. Physiol.* 540, 425–434. [PubMed: 11956333]
- Kim JS, Greene MJ, Zlateski A, Lee K, Richardson M, Turaga SC, Purcaro M, Balkam M, Robinson A, Behabadi BF, et al. ; EyeWriters (2014). Space-time wiring specificity supports direction selectivity in the retina. *Nature* 509, 331–336. [PubMed: 24805243]
- Kittila CA, and Massey SC (1997). Pharmacology of directionally selective ganglion cells in the rabbit retina. *J. Neurophysiol.* 77, 675–689. [PubMed: 9065840]
- Koren D, Grove JCR, and Wei W (2017). Cross-compartmental modulation of dendritic signals for retinal direction selectivity. *Neuron* 95, 914–927.e4. [PubMed: 28781167]
- Lamotte d’Incamps B., Ascher P, and Ascher P (2008). Four excitatory postsynaptic ionotropic receptors coactivated at the motoneuron-Renshaw cell synapse. *J. Neurosci.* 28, 14121–14131. [PubMed: 19109494]
- Lee S, Kim K, and Zhou ZJ (2010). Role of ACh-GABA cotransmission in detecting image motion and motion direction. *Neuron* 68, 1159–1172. [PubMed: 21172616]

- Lee S, and Zhou ZJ (2006). The synaptic mechanism of direction selectivity in distal processes of starburst amacrine cells. *Neuron* 51, 787–799. [PubMed: 16982423]
- Léna C, Changeux JP, and Mulle C (1993). Evidence for “preterminal” nicotinic receptors on GABAergic axons in the rat interpeduncular nucleus. *J. Neurosci.* 13, 2680–2688. [PubMed: 8501532]
- Mataruga A, Kremmer E, and Müller F (2007). Type 3a and type 3b OFF cone bipolar cells provide for the alternative rod pathway in the mouse retina. *J. Comp. Neurol.* 502, 1123–1137. [PubMed: 17447251]
- Matsumoto A, Briggman KL, and Yonehara K (2019). Spatiotemporally asymmetric excitation supports mammalian retinal motion sensitivity. *Curr. Biol.* 29, 3277–3288.e5. [PubMed: 31564498]
- Matsumoto A, Agbariah W, Nolte SS, Andrawos R, Levi H, Sabbah S, and Yonehara K (2020). Synapse-specific direction selectivity in retinal bipolar cell axon terminals. *BioRxiv*.
- Mazurek M, Kager M, and Van Hooser SD (2014). Robust quantification of orientation selectivity and direction selectivity. *Front. Neural Circuits* 8, 92. [PubMed: 25147504]
- McGehee DS, Heath MJ, Gelber S, Devay P, and Role LW (1995). Nicotine enhancement of fast excitatory synaptic transmission in CNS by presynaptic receptors. *Science* 269, 1692–1696. [PubMed: 7569895]
- Mulle C, Choquet D, Korn H, and Changeux JP (1992). Calcium influx through nicotinic receptor in rat central neurons: its relevance to cellular regulation. *Neuron* 8, 135–143. [PubMed: 1309647]
- Nagel G, Szellas T, Huhn W, Kateriya S, Adeishvili N, Berthold P, Ollig D, Hegemann P, and Bamberg E (2003). Channelrhodopsin-2, a directly light-gated cation-selective membrane channel. *Proc. Natl. Acad. Sci. USA* 100, 13940–13945. [PubMed: 14615590]
- Nikonov SS, Kholodenko R, Lem J, and Pugh EN Jr. (2006). Physiological features of the S- and M-cone photoreceptors of wild-type mice from single-cell recordings. *J. Gen. Physiol.* 127, 359–374. [PubMed: 16567464]
- Oesch NW, and Taylor WR (2010). Tetrodotoxin-resistant sodium channels contribute to directional responses in starburst amacrine cells. *PLoS ONE* 5, e12447. [PubMed: 20805982]
- Ozaita A, Petit-Jacques J, Völgyi B, Ho CS, Joho RH, Bloomfield SA, and Rudy B (2004). A unique role for Kv3 voltage-gated potassium channels in starburst amacrine cell signaling in mouse retina. *J. Neurosci.* 24, 7335–7343. [PubMed: 15317859]
- Palazzolo MJ, Hamilton BA, Ding DL, Martin CH, Mead DA, Mierendorf RC, Raghavan KV, Meyerowitz EM, and Lipshitz HD (1990). Phage lambda cDNA cloning vectors for subtractive hybridization, fusion-protein synthesis and Cre-loxP automatic plasmid subcloning. *Gene* 88, 25–36. [PubMed: 2140336]
- Park SJ, Kim IJ, Looger LL, Demb JB, and Borghuis BG (2014). Excitatory synaptic inputs to mouse on-off direction-selective retinal ganglion cells lack direction tuning. *J. Neurosci.* 34, 3976–3981. [PubMed: 24623775]
- Pei Z, Chen Q, Koren D, Giammarinaro B, Acaron Ledesma H., and Wei W (2015). Conditional knock-out of vesicular GABA transporter gene from starburst amacrine cells reveals the contributions of multiple synaptic mechanisms underlying direction selectivity in the retina. *J. Neurosci.* 35, 13219–13232. [PubMed: 26400950]
- Poleg-Polsky A, and Diamond JS (2016). Retinal circuitry balances contrast tuning of excitation and inhibition to enable reliable computation of direction selectivity. *J. Neurosci.* 36, 5861–5876. [PubMed: 27225774]
- Poleg-Polsky A, Ding H, and Diamond JS (2018). Functional compartmentalization within starburst amacrine cell dendrites in the retina. *Cell Rep.* 22, 2898–2908. [PubMed: 29539419]
- Reed BT, Amthor FR, and Keyser KT (2002). Rabbit retinal ganglion cell responses mediated by alpha-bungarotoxin-sensitive nicotinic acetylcholine receptors. *Vis. Neurosci.* 19, 427–438. [PubMed: 12511076]
- Reed BT, Keyser KT, and Amthor FR (2004). MLA-sensitive cholinergic receptors involved in the detection of complex moving stimuli in retina. *Vis. Neurosci.* 21, 861–872. [PubMed: 15733341]

- Séguéla P, Wadiche J, Dineley-Miller K, Dani JA, and Patrick JW (1993). Molecular cloning, functional properties, and distribution of rat brain alpha 7: A nicotinic cation channel highly permeable to calcium. *J. Neurosci.* 13, 596–604. [PubMed: 7678857]
- Sethuramanujam S, McLaughlin AJ, deRosenroll G, Hoggarth A, Schwab DJ, and Awatramani GB (2016). A Central Role for Mixed Acetylcholine/GABA Transmission in Direction Coding in the Retina. *Neuron* 90, 1243–1256. [PubMed: 27238865]
- Sethuramanujam S, Yao X, deRosenroll G, Briggman KL, Field GD, and Awatramani GB (2017). “Silent” NMDA synapses enhance motion sensitivity in a mature retinal circuit. *Neuron* 96, 1099–1111.e3. [PubMed: 29107522]
- Shekhar K, Lapan SW, Whitney IE, Tran NM, Macosko EZ, Kowalczyk M, Adiconis X, Levin JZ, Nemes J, Goldman M, et al. (2016). Comprehensive classification of retinal bipolar neurons by single-cell transcriptomics. *Cell* 166, 1308–1323.e30. [PubMed: 27565351]
- Siebert S, Scherf BG, Del Punta K, Didkovsky N, Heintz N, and Roska B (2009). Genetic address book for retinal cell types. *Nat. Neurosci.* 12, 1197–1204. [PubMed: 19648912]
- Smith RG (1992). NeuronC: a computational language for investigating functional architecture of neural circuits. *J. Neurosci. Methods* 43, 83–108. [PubMed: 1405746]
- Stanchev D, and Sargent PB (2011).  $\alpha$ 7-Containing and non- $\alpha$ 7-containing nicotinic receptors respond differently to spillover of acetylcholine. *J. Neurosci.* 31, 14920–14930. [PubMed: 22016525]
- Stincic T, Smith RG, and Taylor WR (2016). Time course of EPSCs in on-type starburst amacrine cells is independent of dendritic location. *J. Physiol.* 594, 5685–5694. [PubMed: 27219620]
- Strauss S, Korympidou MM, Ran Y, Franke K, Schubert T, Baden T, Berens P, Euler T, and Vlasits AL (2021). Center-surround interactions underlie bipolar cell motion sensing in the mouse retina. *bioRxiv*, 2021.05.31.446404.
- Tang JC, Rudolph S, Dhande OS, Abaira VE, Choi S, Lapan SW, Drew IR, Drokhlyansky E, Huberman AD, Regehr WG, and Cepko CL (2015). Cell type-specific manipulation with GFP-dependent Cre recombinase. *Nat. Neurosci.* 18, 1334–1341. [PubMed: 26258682]
- Taylor WR, and Vaney DI (2002). Diverse synaptic mechanisms generate direction selectivity in the rabbit retina. *J. Neurosci.* 22, 7712–7720. [PubMed: 12196594]
- Tukker JJ, Taylor WR, and Smith RG (2004). Direction selectivity in a model of the starburst amacrine cell. *Vis. Neurosci.* 21, 611–625. [PubMed: 15579224]
- Vernino S, Amador M, Luetje CW, Patrick J, and Dani JA (1992). Calcium modulation and high calcium permeability of neuronal nicotinic acetylcholine receptors. *Neuron* 8, 127–134. [PubMed: 1370370]
- Vlasits AL, Morrie RD, Tran-Van-Minh A, Bleckert A, Gainer CF, DiGregorio DA, and Feller MB (2016). A role for synaptic input distribution in a dendritic computation of motion direction in the retina. *Neuron* 89, 1317–1330. [PubMed: 26985724]
- Wang YV, Weick M, and Demb JB (2011). Spectral and temporal sensitivity of cone-mediated responses in mouse retinal ganglion cells. *J. Neurosci.* 31, 7670–7681. [PubMed: 21613480]
- Wässle H, Puller C, Müller F, and Haverkamp S (2009). Cone contacts, mosaics, and territories of bipolar cells in the mouse retina. *J. Neurosci.* 29, 106–117. [PubMed: 19129389]
- Wonnacott S, Barik J, Dickinson J, and Jones IW (2006). Nicotinic receptors modulate transmitter cross talk in the CNS: nicotinic modulation of transmitters. *J. Mol. Neurosci.* 30, 137–140. [PubMed: 17192660]
- Wright LL, Macqueen CL, Elston GN, Young HM, Pow DV, and Vaney DI (1997). The DAPI-3 amacrine cells of the rabbit retina. *Vis. Neurosci.* 14, 473–492. [PubMed: 9194315]
- Yan W, Laboulaye MA, Tran NM, Whitney IE, Benhar I, and Sanes JR (2020). Mouse retinal cell atlas: Molecular identification of over sixty amacrine cell types. *J. Neurosci.* 40, 5177–5195. [PubMed: 32457074]
- Yonehara K, Farrow K, Ghanem A, Hillier D, Balint K, Teixeira M, Jüttner J, Noda M, Neve RL, Conzelmann KK, and Roska B (2013). The first stage of cardinal direction selectivity is localized to the dendrites of retinal ganglion cells. *Neuron* 79, 1078–1085. [PubMed: 23973208]
- Yoshida K, Watanabe D, Ishikane H, Tachibana M, Pastan I, and Nakanishi S (2001). A key role of starburst amacrine cells in originating retinal directional selectivity and optokinetic eye movement. *Neuron* 30, 771–780. [PubMed: 11430810]

- Zhou ZJ, and Lee S (2008). Synaptic physiology of direction selectivity in the retina. *J. Physiol.* 586, 4371–4376. [PubMed: 18617561]
- Zucker CL, Nilson JE, Ehinger B, and Grzywacz NM (2005). Compartmental localization of gamma-aminobutyric acid type B receptors in the cholinergic circuitry of the rabbit retina. *J. Comp. Neurol.* 493, 448–459. [PubMed: 16261535]

Author Manuscript

Author Manuscript

Author Manuscript

Author Manuscript

**Highlights**

- Retinal bipolar cells express  $\alpha 7$  or non- $\alpha 7$ -nAChRs in a type-dependent manner
- Cholinergic feedback to bipolar cell  $\alpha 7$ -nAChRs boosts SAC direction selectivity
- Bipolar cell  $\alpha 7$ -nAChRs boost asymmetric inhibition to motion-sensing ganglion cells
- Conditional  $\alpha 7$ -knockout from bipolar cells impairs retinal motion detection

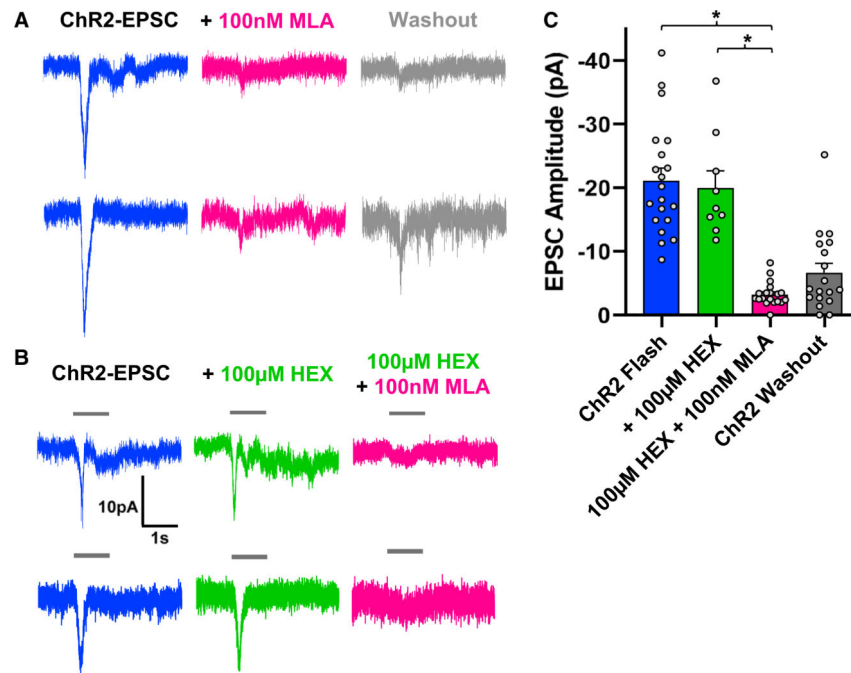


**Figure 1. ChR2-evoked EPSCs in some bipolar cells were MLA sensitive**

(A) In the presence of AMPA, kainite, and mGluR6 glutamate receptor blockers, ChR2-evoked EPSCs were recorded from bipolar cells. Averaged traces are shown for Off (top) and On (bottom) bipolar cells, in which EPSCs were blocked by application of MLA (100 nM, magenta).

(B) In other bipolar cells, we first applied HEX (100  $\mu$ M, green) that did not block ChR2-EPSCs, which were subsequently blocked by application of 100 nM of MLA.

(C) A summary graph of ChR2-evoked EPSC amplitude in MLA-sensitive bipolar cells, which were insensitive to HEX but were blocked by MLA ( $p = 0.0001$ , mixed-model ANOVA). ChR2-evoked EPSCs returned after washout in some bipolar cells (gray). Data are represented as means  $\pm$  SEM.

See also Table S1.

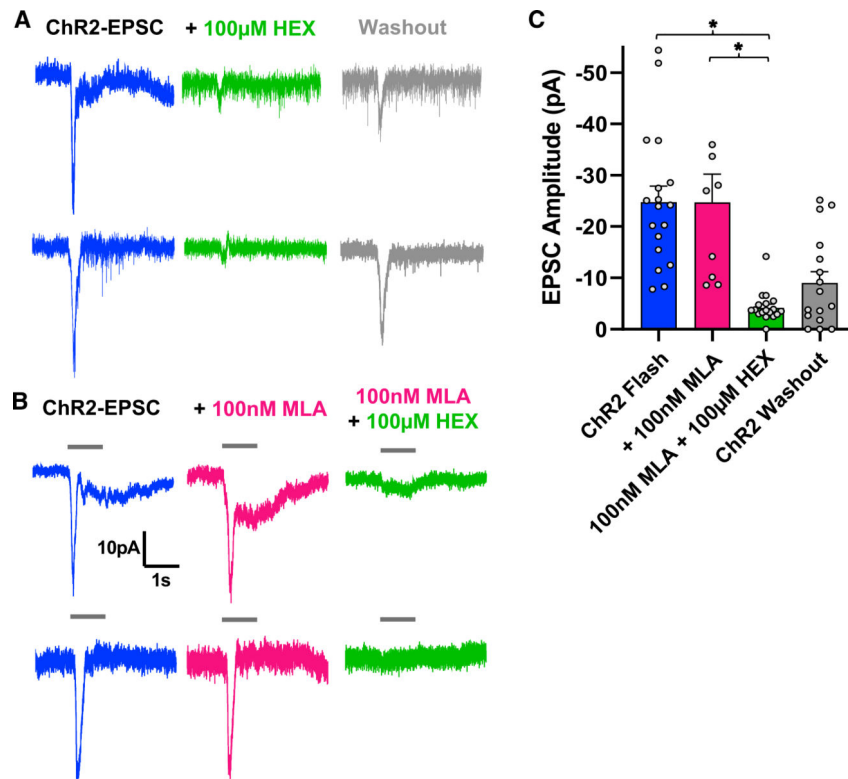


**Figure 2. ChR2-evoked EPSCs in some bipolar cells were HEX sensitive**

(A) In On and Off bipolar cells, ChR2-evoked EPSCs were blocked by application of HEX.

(B) In other recordings, ChR2-EPSCs were unaffected by MLA but were HEX sensitive.

(C) A summary graph of ChR2-evoked EPSC amplitude in HEX-sensitive bipolar cells.

ChR2-evoked EPSCs were insensitive to MLA but were blocked by HEX ( $p = 0.0091$ , mixed-model ANOVA). ChR2-evoked EPSCs returned after washout in some bipolar cells (gray). Data are represented as means  $\pm$  SEM.

See also Table S1.

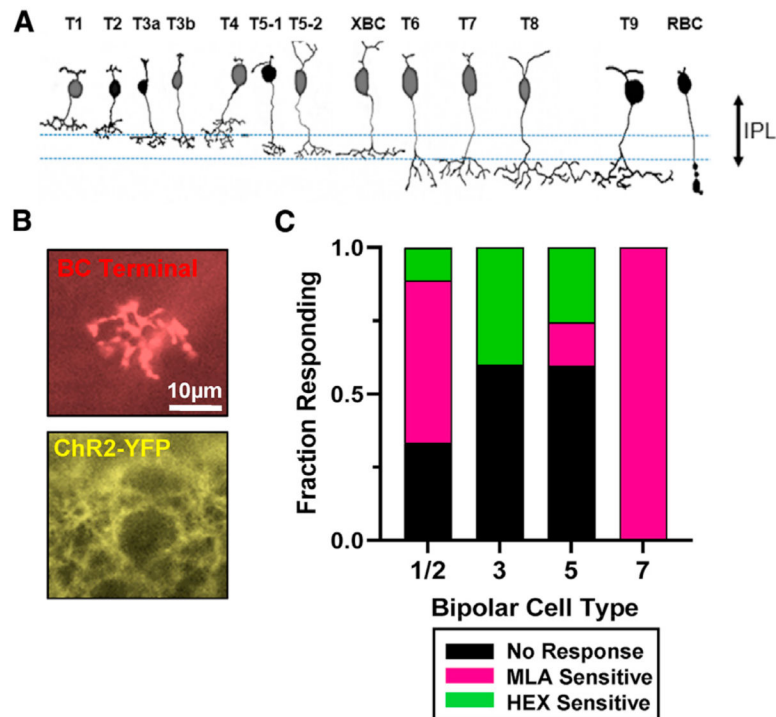


**Figure 3. A summary of ChR2-evoked EPSCs in bipolar cells**

(A) 13 types of mouse bipolar cells project to different IPL depths shown in the retinal slice preparation. The dashed blue lines represent the Off-ChAT (top) or On-ChAT (bottom) bands. Types-1/2 and -3 Off bipolar cells stratify just above or below the Off-ChAT band, respectively. Types 5 or 7 On bipolar cells stratify just above or below the ON-ChAT band, respectively.

(B) A representative HEX-sensitive type-5 bipolar cell filled with sulphorhodamine-B (red) was identified by its axon terminal that stratified at the level of the On-ChAT band (YFP, yellow).

(C) A summary graph showing the fraction of each bipolar cell type that showed no ChR2-evoked EPSCs (black), EPSCs sensitive to MLA (magenta), or EPSCs sensitive to HEX (green).

See also Figure S2.

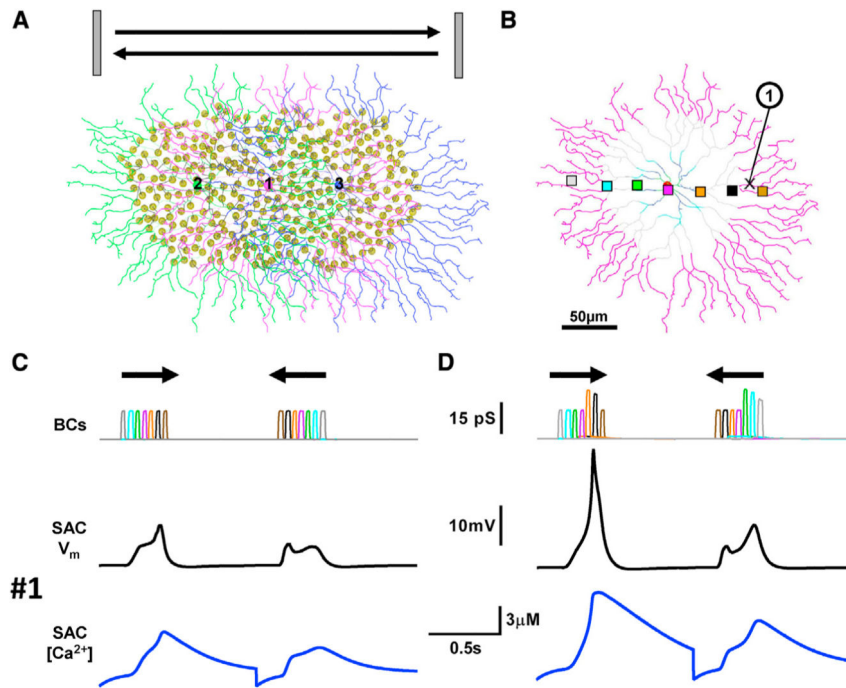


**Figure 4. A 3-SAC model reveals that cholinergic feedback to bipolar cells enhances the SAC centrifugal direction selectivity**

(A) A 3-SAC model based on the digitized morphology of a tracer-labeled SAC. A simulated moving bar (20 μm wide by 400 μm tall) moved left to right, then right to left at a speed of 600 μm/s.

(B) The simulated moving bar depolarized presynaptic bipolar cells (colored squares), which evoked EPSPs and calcium responses in the central SAC. Direction selectivity of motion responses was measured in the right-facing dendrites (point 1). Different dendritic compartments are shown by each color.

(C) Without nicotinic feedback, a bar moving left to right evoked slightly larger EPSPs and calcium responses than for right to left motion, exhibiting weak direction selectivity.

(D) With nicotinic feedback, the EPSPs and calcium response for motion from left to right were significantly enhanced, whereas motion from right to left evoked small EPSPs from signal backpropagation.

See also Table S2.

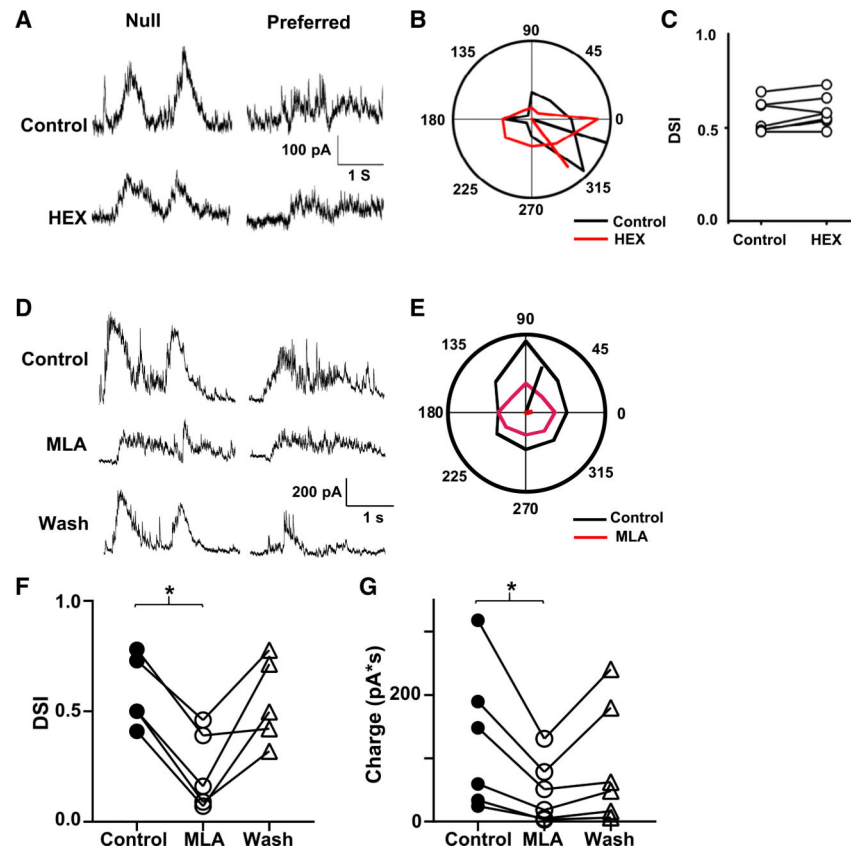


**Figure 5. MLA, but not HEX, reduced the direction selectivity and charge transfer of IPSCs in On-Off DSGCs**

(A) IPSCs were recorded in response to moving stimuli of 100% contrast. Hexamethonium (HEX, 100  $\mu$ M) was applied to block non- $\alpha$ 7 nicotinic receptors. In the presence of HEX, IPSCs were still direction selective.

(B) A radar plot to show direction selectivity in the presence (red) and absence (black) of HEX.

(C) DSI did not change by the HEX application, suggesting that HEX-sensitive receptors in bipolar cells did not have a role in direction selectivity in DSGCs.

(D) IPSCs were recorded from an On-Off DSGC. An  $\alpha$ 7-nAChR antagonist, MLA (100 nM), was applied in the bath, which reduced the IPSCs. The effect of MLA was washed out.

(E) A radar plot showing direction selectivity before (black) and after (red) the MLA application. MLA reduced the direction selectivity, shown by the vector length difference.

(F) DSI of IPSCs (100% contrast) was significantly reduced, which was washed out ( $p < 0.05$ , repeated-measures ANOVA).

(G) Charge transfer for the null-IPSCs was also significantly reduced by MLA application, which was washed out in some cells ( $p < 0.05$ , repeated-measures ANOVA).

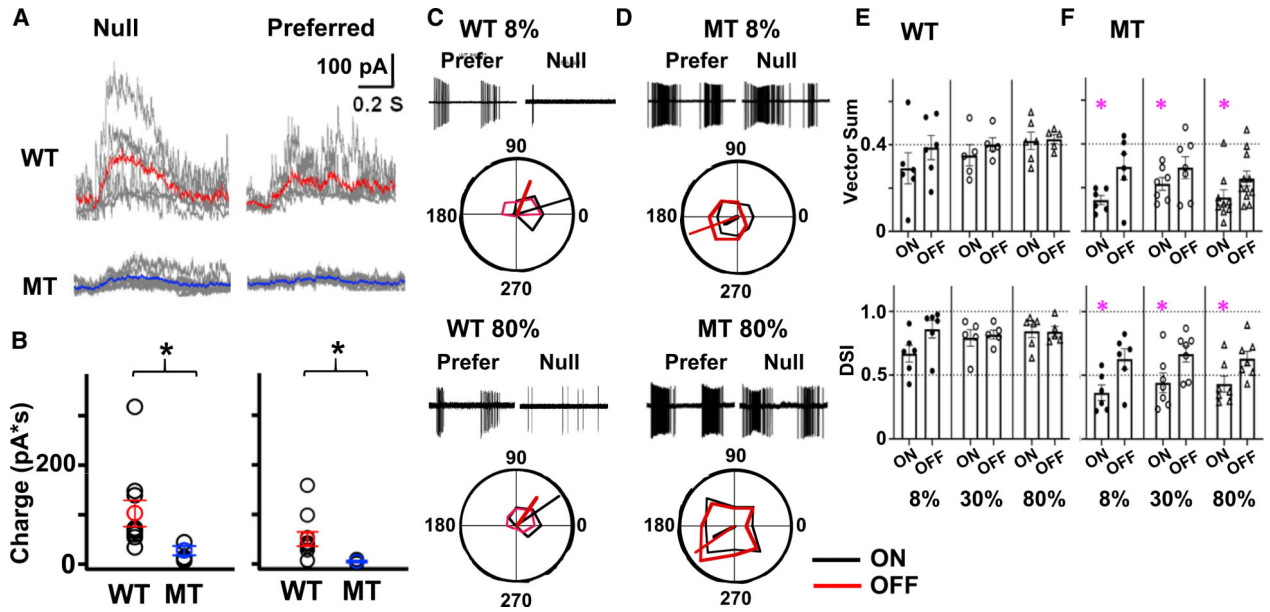


**Figure 6. Direction selectivity in On-Off DSGCs was reduced after  $\alpha 7$ -nAChRs were eliminated from type-7 bipolar cells**

(A) In wild-type mice (WT), On IPSCs were larger in response to null than preferred directional stimuli. IPSCs from individual DSGCs are shown in gray ( $n = 6$  cells), and the average of these traces shown in red. In mutant-type (MT) mice both null and preferred stimuli-evoked IPSCs were reduced ( $n = 6$  cells). The average of traces is shown in blue.

(B) Summary graphs show the charge transfer of IPSCs in WT and MT. Both null- and preferred-evoked IPSCs were significantly reduced in mutant mice compared with WT. Data are represented as mean  $\pm$  SEM.

(C) Spike recording was conducted from an On-Off DSGC in wild-type retina. Direction selectivity was clearly present in response to 8%- and 80%-contrast moving stimuli.

(D) The same recording was conducted from an On-Off DSGC in the type-7  $\alpha 7$ -knockout (KO) mutant-type (MT) mouse. Spike activity was increased, and direction selectivity was reduced.

(E) Summary graphs show the vector sum and DSI in wild-type mice (WT). Both parameters were high for all the stimuli, from 8 to 80% contrast, and ON and OFF responses. Data are represented as mean  $\pm$  SEM.

(F) Both the vector sum and DSIs in mutant mice were reduced. Compared with the WT DSGCs, both parameters for On responses recorded in response to 8%-, 30%-, and 80%-contrast stimuli were significantly reduced (\*). However, Off responses did not exhibit significant differences between wild-type and mutant mouse DSGCs.

See also Figures S3, S4, and S5. Data are represented as mean  $\pm$  SEM.

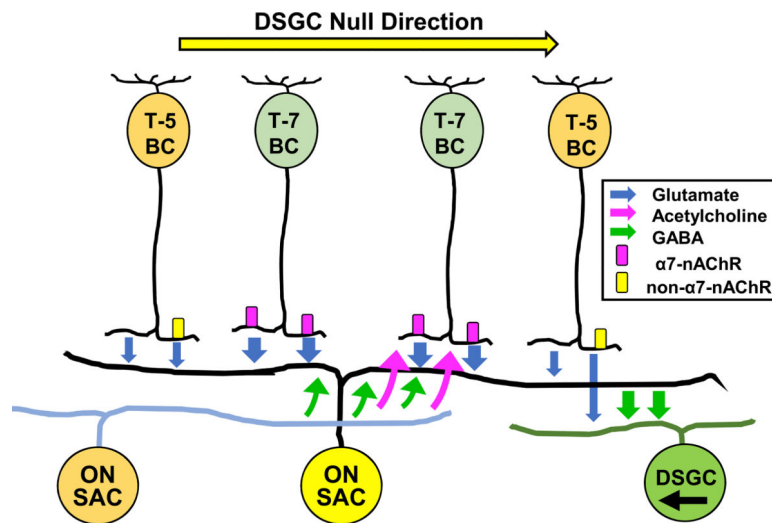


**Figure 7.  $\alpha 7$ -nAChRs in bipolar cells contribute to SAC and DSGC direction selectivity**  
 For an object moving from left to right, the neighbor SAC simultaneously provides lateral inhibition to the primary SAC as well as cholinergic excitation to  $\alpha 7$ -nAChRs in type-7 bipolar cells. This augments the proximal glutamate inputs to the primary SAC, enhancing the SAC distal dendrite's response to centrifugal motion (from left to right here) and GABAergic output for the DSGC-null direction. The lateral inhibition from the neighbor SAC, as well as SAC dendrite compartmentalization, prevents backpropagation of the enhanced glutamate inputs for centripetal stimulation of the left-facing SAC dendrite.

## KEY RESOURCES TABLE

REAGENT or RESOURCE	SOURCE	IDENTIFIER
Antibodies		
Goat anti-choline acetyltransferase (ChAT); monoclonal	Millipore-Sigma	Cat#AB144P; RRID: AB_2079751
$\alpha$ -Bungarotoxin, Alexa Fluor 555 conjugate	Invitrogen	Cat# B35451; RRID: AB_2617152
Neurobiotin Tracer	Vector Laboratories	Cat# SP-1120-20; RRID: AB_2336606
Streptavidin, Alexa Fluor 488 conjugate	ThermoFisher	Cat# S32354; RRID: AB_2315383
Rabbit anti-cocaine and amphetamine related transcript (CART); polyclonal	Phoenix Pharmaceuticals	Cat# H-003-62; RRID: AB_2313614
Rabbit anti-dsRed	Clontech	Cat#632496; RRID: AB_10013483
Donkey anti-rabbit Alexa 488	Invitrogen	Cat#A21202; RRID: AB_141607
Donkey anti-goat Alexa 633	Invitrogen	Cat#A31083; RRID: AB_2535739
Donkey anti-rabbit Alexa 568	Invitrogen	Cat#A10042; RRID: AB_2534017
Bacterial and Virus Strains		
B120 AAV2/8.EF1a.C-CreintG WPRE.hGH	The Schepens Eye Research Institute Gene Transfer Vector Core	N/A
B121 AAV2/8.EF1a.N-CreintcintG WPRE.Hgh	The Schepens Eye Research Institute Gene Transfer Vector Core	N/A
AAV2 7m8-CAG-N-CreDOG-WPRE	Virovek	N/A
AAV2 7m8-CAG-C-CreDOG-WPRE	Virovek	N/A
AAV2 7m8-FLEX-tdTomato	Virovek	N/A
Chemicals, peptides, and recombinant proteins		
Ames' Media	Millipore-Sigma	Cat#A1420-10X1L
Lidocaine N-ethyl bromide	Millipore-Sigma	Cat#L5783 Cas#21306-56-9
L-AP4	Tocris	Cat#0103 Cas#23052-81-5
ACET	Tocris	Cat#2728 Cas#936095-50-0
GYKI53655 hydrochloride	Tocris	Cat#2555 Cas#143692-48-2
Methyllycaconitine Citrate	Tocris	Cat#1029 Cas#351344-10-0
Hexamethonium Bromide	Tocris	Cat#4111 Cas#55-97-0
Deposited data		
Figure 4 SAC Bipolar Cell Simulation	This paper	DOI: <a href="https://doi.org/10.5281/zenodo.5676260">https://doi.org/10.5281/zenodo.5676260</a>
Experimental models: Organisms/strains		
C57BL/6J	Jackson Labs	RRID: IMSR_JAX:000664
B6.129S- <i>Chat</i> <sup>tm1(cre)Low1</sup> /MwarJ	Jackson Labs	RRID: IMSR_JAX:031661
B6.Cg- <i>Gt(ROSA)26Sor</i> <sup>tm32(CAG-COP4*H134R-EYFP)Hze/J</sup>	Jackson Labs	RRID: IMSR_JAX:024109
B6(Cg)- <i>Chrm7</i> <sup>tm1.1Ehs</sup> /YakeJ	Jackson Labs	RRID: IMSR_JAX:026965
STOCK Tg(Gnat3-GFP)1Rfm/ChowJ	Jackson Labs	RRID: IMSR_JAX:026704

REAGENT or RESOURCE	SOURCE	IDENTIFIER
Recombinant DNA		
pCAG-C-CreintG	AddGene	RRID: Addgene_69573
pCAG-N-CretrcintG	AddGene	RRID: Addgene_69572
pAAV-FLEX-tdTomato	AddGene	RRID: Addgene_28306
Software and algorithms		
MATLAB	MathWorks	<a href="https://www.mathworks.com/">https://www.mathworks.com/</a>
SigmaPlot14.5	Systat Software	<a href="https://systatsoftware.com/">https://systatsoftware.com/</a>
pClamp10.7	Molecular Devices	<a href="https://www.moleculardevices.com/">https://www.moleculardevices.com/</a>
AutoQuantX3	Media Cybernetics	<a href="https://www.mediacy.com/autoquantx3/">https://www.mediacy.com/autoquantx3/</a>
NEURON-C	(Smith, 1992)	RRID: SCR_004275
GraphPad Prism 9	GraphPad	<a href="https://www.graphpad.com/">https://www.graphpad.com/</a>